# UC Irvine
## UC Irvine Electronic Theses and Dissertations

**Title**

Design of Cardiovascular Energy Harvesting Devices

**Permalink**

https://escholarship.org/uc/item/4f44n095

**Author**

Agnew, William James

**Publication Date**

2019

Peer reviewed|Thesis/dissertation

UNIVERSITY OF CALIFORNIA,
IRVINE


Design of Cardiovascular Energy Harvesting Devices


THESIS


submitted in partial satisfaction of the requirements
for the degree of


MASTER OF SCIENCE

in Biomedical Engineering


by


William James Agnew V

Thesis Committee:
Professor William C. Tang, Chair
Assistant Professor Christine King
Associate Professor Anna Grosberg

2019

# DEDICATION

To

Stephanie Chan

For the constant love you have displayed, symbolic of Christ's love.

Psalm 127:1-2 (ESV)

Unless the LORD builds the house, those who build it labor in vain. Unless the LORD watches over the city, the watchman stays awake in vain. It is in vain that you rise up early and go late to rest, eating the bread of anxious toil; for he gives to his beloved sleep.

# TABLE OF CONTENTS

# LIST OF FIGURES

# LIST OF TABLES

# ACKNOWLEDGMENTS

# ABSTRACT OF THE THESIS

Design of Cardiovascular Energy Harvesting Devices

By

William James Agnew V

Master of Science in Biomedical Engineering

University of California, Irvine, 2019

Professor William C. Tang, Chair

Two fields of cardiovascular energy harvesting are investigated, (1) stents and (2) leadless pacemaker. The demand for rechargeable technologies in cardiovascular stents arose from the unmet clinical need for real-time tracking of re-occlusions in implantable stents. This thesis entertains the idea of piezoelectric cantilevers positioned at the inlet/outlets of the stent to harness the pulsatile blood flow within arterial cavities to power wireless communication circuits to notify physicians of plaque growth. A MATLAB study utilizing literature-based blood flow velocities in both healthy and diseased patients yielded 3.5mV energy harvesting potentiality. Then, a large-scale benchtop study successfully produced a simplistic model to see if the pressure differences expected across the stent (.4 Pa). Both tests prove the feasibility of such a design. With a 95% reduction in volume from its predecessors, the leadless pacemaker traded compatibility with battery longevity going from a 10-year device lifetime to 6 years [3,34]. Enclosed is an energy harvesting accessory intended to slip around leadless in-ventricular pacemakers such as the Medtronic Micra. Two designs featured mechanisms to harvest the blood pressure and the ventricular wall force from within the heart cavity via electromagnetic induction by

ferrofluid and solid ring magnets. The team promptly abandoned the ferrofluid mechanism due to its limited induction capabilities after its 20x deficiencies compared to solid core magnets demonstrated by multiple benchtop tests. However, the solid ring magnet design proved successful after meeting eight out of nine acceptance criteria through simulation studies [Modal/Fatigue/Induced Voltage/Heat Generation/Mesh compliance] and benchtop studies [Induced Voltage/Magnet Shielding/Heat Generation].

# Chapter 1 - Introductions

## 1.1 Demand for Cardiovascular Rechargeable Technologies

Two devices characterized the onset of the implantable device era, the renown technologies of the pacemaker and the cardiovascular stent. With over 1,000,000 pacemakers implanted in 2009, the pacemaker till this day remains one of the most impactful implantable devices [1]. Yet, the industry is beset with a critical issue. In 2009, ~26% of total pacemaker surgeries (264,824 of 1,000,000) [1]. The lifetime of these devices is expiring far too rapidly with the root cause being an expired battery cell. Even

Figure 1-1. Medtronic's traditional pacemaker compared against their newest in-ventricular pacemaker a 93% reduction in size [2]

Source: Adapted from [3]

with this known issue, market analysts anticipated that the pacemaker market would eventually shift towards a leadless implantable device into the ventricular cavities of the heart. With the advent of new battery technology, leadless pacemakers created by Medtronic© and St. Jude Medical © are being sold. These devices have an average of six to seven years of lifetime a 40% reduction in usability from the prior model. Likely, this is due to battery constraints that come with the reduction of size from ~12.85 cm3 to .8-1 cm3, a 93% decrease in volume [3,4,5]. Although the average age of a pacemaker implantation is 73.5, the number of patients under the age of 65 diagnosed for cardiac arrhythmias is approximately 6.5 million [6]. Thus, if a patient requires a pacemaker at a younger age, they

have the potentiality of undergoing multiple replacement surgeries each surmounting the risk of surgical casualties.



Figure 1-2. Cardiovascular Stent

Source: Adapted from [7]

Stents hold a massive market, when amalgamated, 2 million implantations occur each year in the U.S and European theater. Practitioners yearn for "smart stents" [8] which may wirelessly communicate with physicians on cardiac output or blood flow metrics. Trading between higher accuracy in data transmission and power consumption weighs on the smart stent, of which its minuscular average diameter of 3 mm and total length of 15.45 mm leaves little room for battery storing capacities [9]. Thus, we turn to the investigation of energy harvesting techniques for cardiovascular stents and for implantable ventricular pacemakers to fulfill the technological demands provided by physicians and patients.

A priori, we encounter the physiological question regarding the efficacy of leaching energy from a closed system. This question requires a series of in-depth clinical long-term

studies; however, as noted by P. Fenniger et al. [10], theoretically this challenge may be dismissed. To prove this theory, we may (1) calculate the current power generation in a human body by blood flow process, (2) determine the necessary power for either an in-ventricular pacemaker or wireless stent, and (3) compare the two. In Fluids: Human Cardiovascular System, Koehler, begins with the assumption that the power output of the heart is the product of the pressure multiplied by the volumetric flow [11]. It then follows, "If you have six liters of blood and it circulates every minute, the flow rate is 100 cm3/s. If the pressure averages 133,000 dynes/cm2 (ignoring pulsatile flow), then the average power output is 13,300,000 ergs/s or 1.33 watts [11]".

P. Fenninger adds that incorporating the pulsatile nature of the heart would increase this total power production by 25% [10], thus reaching 1.66 W. Returning to the literature once more, the next question raised is how much power is required for sustaining a long-term pacemaker? Luckily, several groups have agreed upon a collective amount of approximately 10 μW production [12]. Even if there was a 100% loss in efficiency by other variables, such as the mechanical variables, heat and acoustics (though noted to be only approximately 8% of normal losses) and adding a 3x scaling for potential greater energy needs in the future thereby accounting for inefficiencies in the recharging system[13]. The conclusion, then is that a 60uW of re-directed energy would be consumed, a paltry amount of 0.0036%. Still, even such a finite amount of energy drawn from the cardiovascular system could destabilize the body, thus further work will be taken to investigate into this potential failure mode.

1.2 Energy Harvesting Applications: Stent Occlusion Diagnosis and In-Ventricle

Therefore, with the demand for energy harvesting technology and the energy loss phenomena addressed, the methods of energy harvesting possible for the stent and pacemaker are discussed. P. Fenniger organizes the categories for energy harvesting into four primary niches: (1) heart motion, (2) pressure gradients, (3) blood flow and (4) arterial compliance [10]. Heart motion utilizes the large ventricular volume displacement (~20%) and mechanical wringing motion created by the pulsatile pump consisting of the ventricles and atriums. Further, pressure gradient between systolic (120 mmHg) to diastolic (80-85 mmHg) allows for the enactment of differing mechanical transducers to convert such a differential to usable energy. Blood flow velocity, or the speed at which the blood flows, is another alternative where it has been cited that aortic flow rates may peak at 1.2 m/s [10]. Lastly, the arterial wall compliant nature allows for rapid dilation or volumetric increases during systolic pressure cycles and decompression during low pressure, allowing for possible energy harvesting . In particular, the two methods outlined in the chapters to follow focused on the first two niches mentioned, heart motion and pressure gradients. As a simplified overview, one project consisted of investigating a blood flow sensor stent which utilizes the pressure gradient created within the bloodstream to contract piezoelectric cantilevers with nitinol cores. In turn, this deformation triggers a voltage output within the circuit which may be used for diagnostic or energy harvesting purposes. One case includes charging a wireless communication unit anchored to the stent, altered by the blood flow sensor itself to notify physicians if underlying symptoms have altered. While this project continued, a secondary project emerged which utilized the pressure-driven momentum of the blood within the ventricle to displace ferrofluid to

generate an electrical charge. However, after significant studies, this process was abandoned for the former niche, such that by utilizing the heart walls, greater force is applied to the energy harvester, which translates into higher energy outputs.

## 1.3 Prior Research – Stent Occlusion Diagnosis/Energy Harvesting

This design has two components: (1) a novel stent occlusion diagnosis, and (2) the energy harvesting capabilities for the stent diagnosis communication.

After implanting a stent, reocclusion of coronary arteries presents a severe risk, with thrombosis frequently occurring in 30 days (1%) the 0.2-0.6% within the year and 0.5-0.6% after four years [14]. It has been noted that with bare metal stents, the rates of thrombosis occurring may be even higher at 5.6% of the total patient survey as seen in Wilson et al. [15]. Detection of these events normally requires a patient to see their physician and proceed with an angiography or x-ray of the at-risk location. By Bernoulli's equation [16]:

$$p_1 - p_2 = \frac{1}{2}\rho(V_2^2 - V_1^2) \tag{1.1}$$

$$\text{and } A_1 V_1 = A_2 V_2 \tag{1.2}$$

Therefore,

$$A_2 < A_1, V_2 > V_1 \tag{1.3}$$

$$V_2 > V_1, p_2 < p_1 \tag{1.4}$$

At the onset of a plaque buildup the cross-sectional area for blood flow will decrease, thus causing a differential in velocities between the two sections. This

elementary theory then creates the backdrop for the common blood flow sensor technology to determine potential thrombosis events.
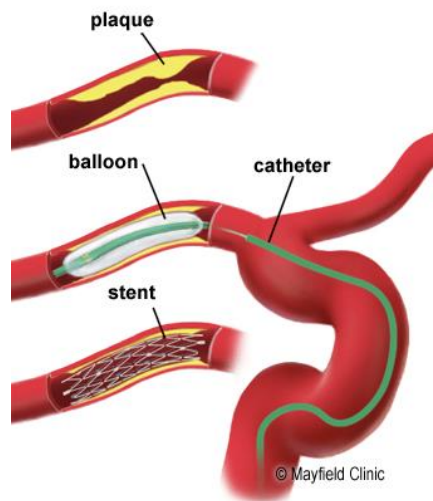


Figure 1-3. Balloon expandable cardiovascular stent implantation methodology.

Source: Adapted from [17]

Other methods of blood flow sensing include ultrasonic sensors have been used to measure and understand flow and can be especially useful since they are highly accurate, have rapid response, and are not affected by any variations in properties of the fluid such as pressure, temperature, and viscosity. These sensors can be especially useful in healthcare because some types do not require invasive surgeries to be used. There are four main types of ultrasonic blood flow sensors: transit-time, pulsed Doppler, laser Doppler flow meter, and continuous-wave Doppler flow meter. Each uses different methods to find the velocity of fluid through a specific area [18]. Transit-time uses a transmitted sound and uses the time difference between the transmitted and received sounds, but one downside is that it requires invasive surgery to use. The pulsed Doppler acts like a radar and uses pulses and the received signals to determine the velocity of the fluid by the changes in delay between transmittance and receiving the signal. The laser Doppler flow meter uses a

6

shift in light caused by red blood cells to find velocity. The existing research created a device that could measure flow using a signal generator chip that provides a signal, and then gets amplified, and then mixed with the receiving signal. This led to two signals, one being a sinusoidal signal that was Doppler shifted. The shifted signal was analyzed using MatLab and spectrograms along with a low pass filter to find the velocity. The project was successful in finding a positive correlation between increase in flow velocity and magnitude of audio signal, but further testing was required to compare with existing results and refining the device for maximum accuracy [18].

US Patent No. 5.409,009 details a sensor that measures arterial blood flow. In this specific device, two electrodes on a transvenous lead body within the vein is adjacent to the artery that is being used to measure the variations in impedance of the blood between the electrodes. By positioning the sensor in the adjacent vein and using the piezoelectric effect it can generate electrical charge when mechanical stress is applied. This sensor allows for measuring of arterial blood pressure pulses, and acts as a flow sensor [19].

As for energy harvesting applications, although it has been noted that the natural human energy harvesting system yields low-power capabilities, with the onset of low power circuits energy harvesting appears an attractive solution for engineers to the battery storage issues [20]. A cursory examination of the research field shows that it is relatively quiet on the subject for charging cardiovascular stents but there were some teams focused on arterial compliance energy harvesters. For instance, Nanda & Karami investigated a device that would be inserted inside an artery. The device was placed near the brain for microsensor charging, and by the dilation of the artery, the adjacent curved energy harvested would also deform [21]. This compressible sleeve would then generate an

electrical output which could be transmitted to nearby sensors for charging. Ideally, this could also be implemented into a stent system where the inner diameter of the stent would come with such a flexible sleeve. However, two concerns arise. First, since stents are often crimped to fit the sizing necessary for coronary or cardiovascular implantation. The insertion diameter would then be as small as 3-9 Fr or 1-3 mm and then balloon-expanded or self-expanded (via nitinol stents) into their final sizing of 3-6mm [22]. This crimping to almost 33% of the original diameter could potentially damage such cylindrical bimorph cantilever, likely made from the polyvinylidene difluoride (PVDF) material to be biocompatible. Considerable damage has been done similarly during crimping and well documented for TAVR heart valves [23]. The second concern is the inability to fit such thickness of the bimorph cylindrical cantilever inside the small inner diameter (less than 1-3mm) of the stent.
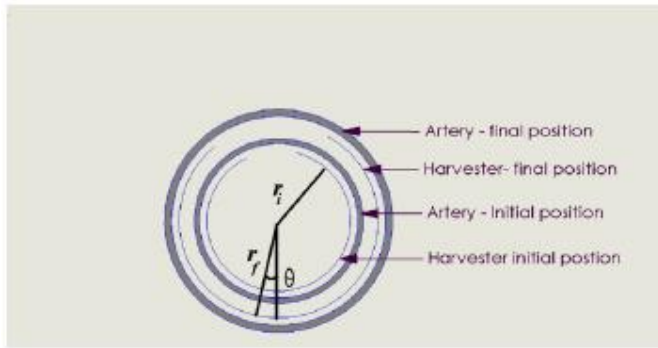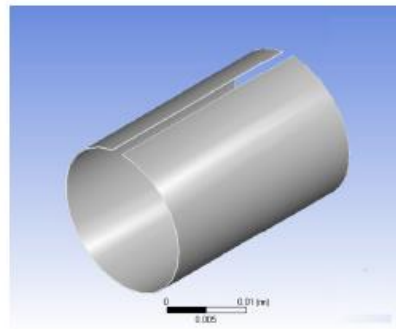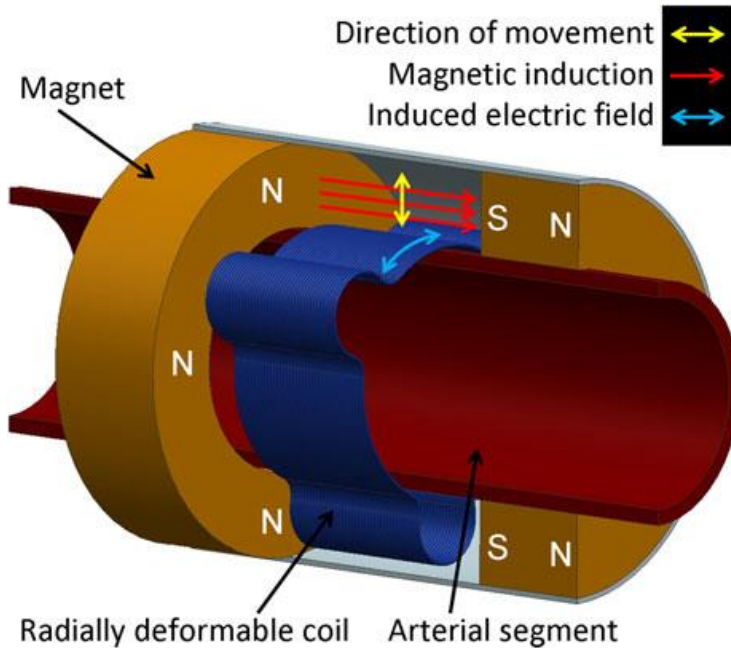
Figure 1-4.Arterial Energy Harvesting Devices.

In A and B, describe a prior work of a cylindrical piezoelectric cantilever design that was completed by Nanda and Karami, which originally was applied for sensors used to monitor cranial activities, yet its application could also potentially be found for cardiovascular stents. A potential failure mode occurs for this design during the stent crimping procedure likely to induce high stress loads on such a device In C, Nagel in 1997 proposed the use of implanting two permanent magnets on an artery which via the dilation of the artery would shift an induction coil thus producing a current.

Source: Adapted from [21,10]

Another idea includes the following, patented by Nagel in 1997 [10], in which two permanent cuff magnets would be stationed on the outside of an arterial segment and a flexible outer sheath with three coil regions (shown in blue in the image). By the coil regions expanding and contracting, an electrical current is induced by the nearby permanent magnets. However, any ideas such as these would require surgical implantation, and would inhibit the utility of such a rechargeable design to today's outpatient surgeries for cardiovascular stents.

## 1.4    Prior Research – Stent Occlusion Diagnosis/Energy Harvesting

Table 1. 1. St. Jude's and Medtronic's Devices the Nanostim & Micra comparisons that provide an overview of geometry, battery lifetime and other important design elements[23, 24]

| Device | Nanostim | Micra |
|---|---|---|
| Dimensions | Diameter: 6 mm, 18 Fr, Length 42mm, Volume 1 mm | Diameter: 6.7 mm, 23 Fr, Length 26mm |
| Volume | Volume: 1 mm3 | Volume: 0.8 mm3 |
| Average Procedural Times | 28 minutes | 37 minutes |
| Battery Life | Estimated battery life of 8.4 years at 100 percent pacing, 12.4 years at 50 percent pacing | Estimated battery life of 4.7 years with 100% at 2.5 V to 14.5 years at 0% pacing. |
| Device Design | "The proximal portion of the device has a docking interface with most of the surface of the device serving as the ring electrode. The distal end has a fixation helix surrounding a tip electrode" (Bernard) | "The anode is a circumferential ring located in the proximal portion of the device, and the cathode is at the tip of the device" (Bernard) |
| Insertion of Device | Can be re-screwed or implanted again if fails pacemaker electrical tests during initial implantation | Implanted and fixated with 4 nitinol tines |
| Removal of the Device | Removed successfully after 3 years from 14 patients | Design allows removal but the device is meant to be an end of life device |

Energy harvesting is not a novel idea for recharging implantable devices. Possible energy harvesting solutions include using thermal differences, electromagnetic induction,

and piezoelectric material electromagnetic induction. We may first rule out the possibility

of using thermal differences inside the heart to create energy, as the body maintains a

nearly constant temperature of 97°F. Thus, such a stable temperature environment lacks a

thermal gradient required for energy harvesting. Previous inventions included large

apparatuses that converted energy via the pulsatile flow of the blood by a series of coils

and pulleys which would oscillate a platform and an attached rectifier and capacitor system

(Figure 1-5) by McLean and Saunders in 1971[26]. Yet with such a large structure, there

comes the complications of size, biocompatibility, patient comfort, and incompatibility with

leadless technology. Mclean's device would be infeasible due to its size and to the increased

opportunity for a biological rejection or fibrous cap formation which may inhibit the

mechanism [26]. Also, patient comfort would also most likely be decreased as the

noticeable apparatus would require surgical implantation and perhaps cause irritation due

to large size. Finally, the size of the mechanical device would inhibit its implantation into

the ventricular cavity of the heart necessary to attach to the new leadless technology

mentioned above. It could require excessive surgery to maneuver such leads through the

cardiac system. Inventors, Irani, et al. recently created a similarly large scale device that

harnessed the hemodynamic blood flow and magnetic induction (Figure 1-5). To solve the

issue of size, MEMs (micro-electrical mechanical systems) offer a desirable alternative. In

one patent, the team of Kotha et al. investigated the idea of using a magnetic fluid inside a

MEMs device which would include a pump, reservoir, and electric coils inside a tubing

housing [27], in which the magnetic fluid by electromagnetic conduction would continue to

be circulated to generate power. There are a few issues with such a design, namely that the

pump would draw excess power away from the recharging system. By the conservation of

energy such a design to "make" energy in such a fashion of using a pump and a magnetic

fluid loop is infeasible as there would be significant energy lost to the environment and

placed into the pumping motor. However, the concept of using such a magnetic fluid is

desirable if the problem of a natural pump could be solved. One team led by Arnold et al.

patented the idea of using a solid magnetic substance which could solve the natural pump

problem (Figure 1-5). However, such a desire fails to utilize the pressure induced force of

the heart, the largest available sources of energy making, MEMs vibrational

electromagnetic induction may be inferior to piezoelectricity [28,29]. MEM's technology

also offers another alternative for energy generation due to piezoelectric materials and

micro-technology machining. Working within this space has been the Inman team who has

developed a non-linear vibrational energy harvester that reacts to heartbeat waveform

movement. Essentially, as the heart beats, this creates a lateral deformation and this

vibrational movement causes the cantilevers to bend, much akin to the shaking of keys

within one's pocket during walking. Although similar to the proposed idea, this

piezoelectric setup has a number of drawbacks, namely, that it does not utilize the 3D

capabilities of piezoelectric, the pressure induced force within the ventricular cavity, and

lastly, its manufacturing procedure and insertion of the magnet components would be

difficult to perform. First, as Iraan et al. has demonstrated in their patent is the usual

piezoelectric MEMs device, as common manufacturing techniques for the micro scale excel

at 2D linear structures. However, this limits the capabilities for energy harvesting by

restricting the design to the two-dimensional plane [28]. By being inside the ventricular

cavity, an energy harvester could now utilize two sources of energy, the heart's vibrations

and the turbulent flow of the blood noted by Irani et al. Third, the manufacturing procedure

to install a singular magnet tip required for the construction of such a device is unrealistic given the constraints of current MEMs fabrication technology and the size of these devices. Furthermore, there are many patents covering the field of using piezoelectric cantilevers. The objective of the following design was to construct an easily manufacturable product which may harvest the pressure induced forces within the ventricular cavity.
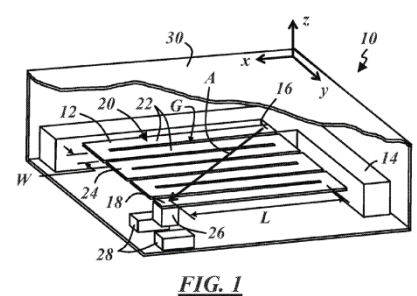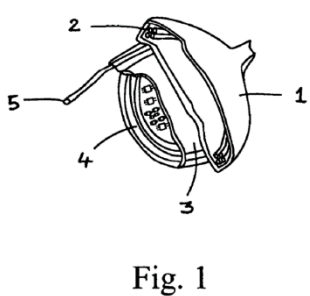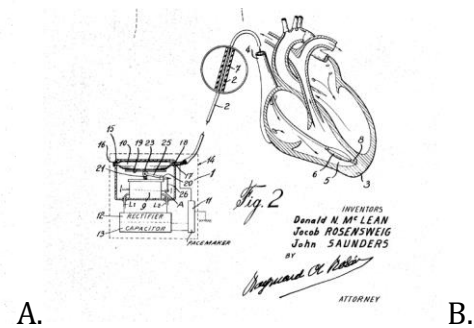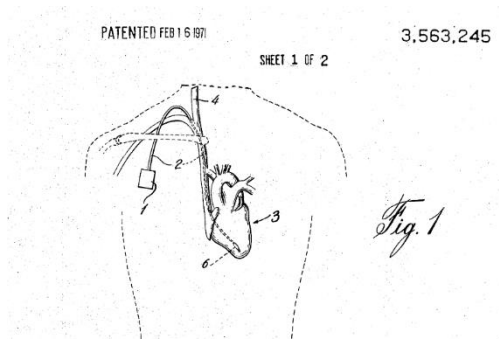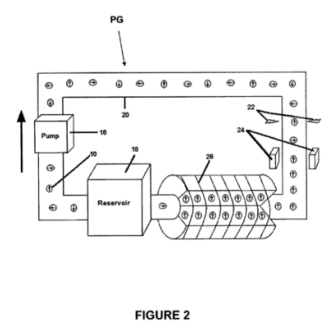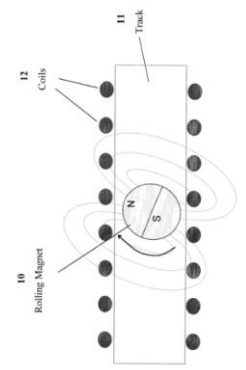
Figure 1-5. Energy Harvesting Patents.

Demonstrating the prior art for the prior patents in the field. A. (1971) Is the large-scale model of the size of the device invented and relative position within the body. B. (1971) Shows the mechanical solution of pulleys and a rocker arm to oscillate thereby creating energy via a rectifier and capacitor. C. (2009) A large, magnetic induction coil-based solution, where the pass blood would generate a force to cause the oscillation of a magnet within a coil, creating an electrical current. D. (2015) A piezoelectric solution utilizing a zig-zag design in order to create electricity. A case for infinite energy where a pump will move a ferrofluid through a series of tube and through an electrical coil to generate electricity, E. A spherical magnet which may pass through a series of coiled loops to generate electricity by the basis of electromagnetic induction [27-30].

1.5     Advantages for Electromagnetic Design and in Heart Design

Instead of using piezoelectric materials, our team focused on the use of ferrofluids/solid ring magnets as the electromotive element inside the energy harvester. Originally invented by NASA as a solution to keep rocket fuel from sloshing around in propellant tanks in zero gravity, ferrofluid has since been employed in the development of technologies such as higher fidelity stereo speakers and semi-active vibration dampers for mechanical and aerospace applications [29] [31]. Ferrofluids are defined as liquids that are strongly magnetized in the presence of a magnetic field. With an external magnetic field, the magnetic dipoles in ferrofluids rotate and produce a net magnetic moment, creating a parallel direction [32]. The parallel direction of the magnetic moment creates the highest output voltage which will generate enough energy to power the pacemaker. Ferrofluids are applied to energy harvesting devices because of their magnetic properties and fluidity, making it easy for them generate electromotive forces even with small vibrations [33,34]. The ability to convert very small amounts of mechanical energy to electrical energy is the primary reason this team has chosen to pursue experimentation with ferrofluid. On the other hand, solid magnets have a proven record to have a notably higher magnetism than possible with ferrofluid. Solid magnets, particularly rare earth magnets, will sustain higher magnetism and induction compared to the ferrofluid or iron based counterparts. Chemically, the electrons in the alloy structurally arranged themselves anisotropically and thus show a higher induction force (Br) and higher resistance to demagnetization. In particular this team utilizes neodymium magnets, which contains primarily the rare earth component neodymium (31% composition)[35]. In summary, magnets offer the largest energy harvesting potential, as they may be scaled directly with the potency of the magnet

chosen and with the size of the magnet, which may be increased relative to the alternative

cantilever size.

A priori deductions on the nature of induced voltage may be analyzed using four

primary equations:

$$P = \frac{V^2}{R}$$ (1.5)

Thus, working backwards from the initial goal, that being a 10 μW power output, a

500 Ω impedance from the Medtronic circuit would need an induced voltage of 5 mV[25**].

This would then be optimized by using the equations below to obtain the various means to

obtain 5 mV. Where $\varepsilon$ is the induced voltage, $B$ the magnetic field, $L$ the length of the coil, $v$

the velocity of the movement of the magnetic field, $I$ the induced current, $R$ the resistance of

the circuit, $\phi$ the magnetic flux, $A$ the cross section area of the coils,  the angle in relation to

the magnetic field, $N$ the number of turns in the coil, and $P$ the power outputted.

$$\varepsilon = BLv,$$ (1.6)

$$\phi = BAcos(\Theta),$$ (1.7)

$$\varepsilon = -N \, \Delta\phi/\Delta t$$ (1.8)

# Chapter 2 - Energy Harvesting for Stent Occlusion Diagnosis

2.1 Design Details

The design concept initiated on the basis of need basics of fluid flow principles.

$$\frac{\partial P}{\partial x} = k_s = \frac{P(L) - P(0)}{L} = \frac{\Delta P}{L} \tag{2.1}$$

$$v_s = \frac{k_s}{4\mu}(r^2 - a^2) \tag{2.2}$$

The above equations are derivations based upon the assumption of a rigid tube, no slip wall conditions, and fully developed fluid flow from the Naiver Stokes equation and the equation of continuity with ks as a constant [16]. If we then rearrange these two equations, we can achieve the simple form of the following:

$$\Delta P = \sigma_{steady\ state} = 4v_{max} * \mu * \frac{L}{a^2} \tag{2.3}$$

Thus, a simple pressure/stress equation is achieved based upon the velocity of the blood within the constructs of the device. The pressure applied onto the cantilevers position at P(0) and P(L) and by the simplification is then translated as noted in Sirohi et al. [36].

$$V = \frac{\sigma dt}{e} \tag{2.4}$$

The voltage created by the pressure sensors is then calculated. This works in two parts, where one element of the design identifies the pressure differential and other provides the utility of generating voltage for the energy harvesting component.
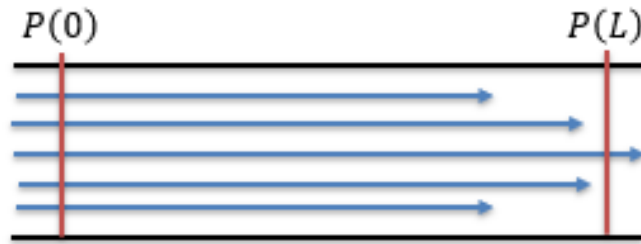
Figure 2-1. Pressure gradients across a rigid tube differ where P (0) > P(L).

Further, blockages located at P(X), where X is some distance between 0 and L will cause the quadratic gradient to increase between the two end points until laminar flow is established.
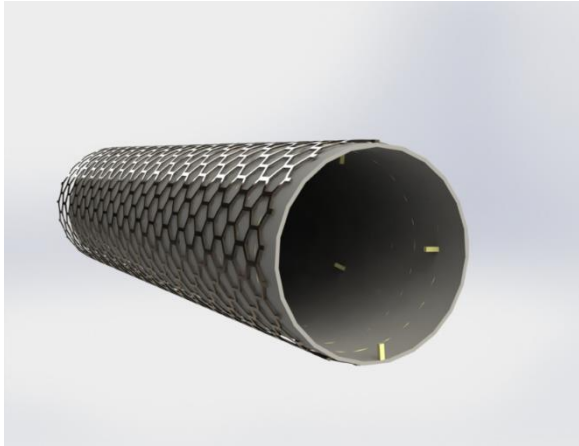
Figure 2-2.Final Design- Stent Occlusion.

The stent occlusion diagnosis and energy harvesting final design complete with inlet/outlet piezoelectric cantilevers which are offset at 30-60 ° increments along the stent.

Having just two piezoelectric cantilevers would justify a blood flow sensor but to augment the recharging capabilities, the team envisions the use of a 360-degree cantilever normal to the surface of an inner wall of a stent at 30-60-degree offsets. These will then maximize the amount of energy harvesting while minimizing the obstruction to the flow path of the blood. Additionally, for a more complete flow profile the voltage signal may be compared between each of these offsets adding to the resolution of the data. The third innovation is the utilization of a nitinol core within each of the piezoelectric cantilevers. The cores will act like a structural beam whose shape memory, described in detail below, will allow the restoration of the PVDF even after crimping events and will increase the lifetime of the beams. Of course, one consideration, is whether the additional structure would cause turbulent flow within the artery. However, it is well known that turbulent flow will diminish into laminar flow given a proper distance. With the long length that the arteries cover within the body we assume that such a disturbance is negligible, yet will be investigated in future studies.

The piezoelectric property is present in few materials. The property allows the material to convert energy between mechanical and electrical forms. Some materials that have this property are some types of ceramics, crystals, quartz, and lead zirconate titanate.

However, these materials are generally brittle and rigid, with lead being poisonous to humans, so none of these materials would be ideal to use in biomedical applications [37]. Piezoelectric polymer polyvinylidene fluoride (PVDF) has applications that are extremely useful in devices such as flow sensors. PVDF is lightweight, flexible, and its piezoelectric voltage constant is about 20 times higher

Figure 2-3. The cantilever design with a PVDF outer sleeve and a Nitinol core.

The Nitinol is incorporated such that it will support the cantilever during the high load event caused by stent crimping.

than that of PZT and 40 times higher than that of Barium titanate, other piezoelectric materials. Additionally, PVDF has a lower density, making it much more suited for biomedical use compared to piezoelectric crystals. The β-phase film of PVDF is one in which the crystalline regions inside the bulk film align in the direction of the electric field. This allows the PVDF to have a higher piezoelectric constant and makes it better suited for use in sensors. Additionally, copolymers of PVDF have higher crystallinity, which have better piezoelectric response, which can be useful when more rigidity is required. The β-phase PVD-TrFE film, a copolymer of PVDF, can operate well in conditions up to 100 °C [38].

Nitinol has a useful property of shape memory. Nitinol is a nickel and titanium alloy, and is widely used in medical applications. Nitinol can remember its shape due to thermoelastic martensitic phase transformation [39]. The nitinol is in martensitic state at

the original temperature, and then when pressure is applied, it changes to detwinned

martensite. Then, when the material is heated to austenite temperature, the original shape

is recovered. This arises when a change in lattice structure occurs by phase transformation

of the material. The transformation temperature is well below or close to body

temperature, so it is ideal to use in biomaterials compared to other materials that have this

property. Another key property of nitinol is superelasticity. In this case, force is applied,

and the austenite transforms to stress induced austenite [39]. When the applied force is

removed, the material reverts to austenite. This property is especially useful in a blood flow

sensor since there will be constant force applied from blood flowing, and the sensor needs

to be able to hold its shape to perform accurately. Due to its high compressive strength and

the properties of shape memory and superelasticity, nitinol is an ideal material to use in

stents.

## 2.2 Simulation Studies

Abstract:

Two "cantilevers" were analytically set up at both the inlet/outlet of a channel, then using blood velocity data gathered from literature along with the equations noted below from Zamir's *The Physics of Pulsatile flow*[16], the voltage and pressure differences were calculated between the two end points. The purpose of this project was thus to prove the feasibility of detecting pressure differences as well as noting the potential voltage generation possible.

Materials and Methods:

To test the conceptual coronary artery flow velocity, mild to moderate stenosis with the normal patient data were adopted from literature and applied as follows. The pressure drop from the beginning to the end of a 15.45 mm stent, the average stent length [9], was calculated based on both a laminar flow model and a pulsatile flow in a rigid tube, with a rigid wall assumption. This pressure drop was then used to calculate the expected voltage difference from two piezoelectric cantilevers made of Polyvinylidene difluoride (PVDF). Cantilevers were considered such that with two boundary plates, assuming a capacitor model [36]. Cantilever geometry was assumed to be: 1000 x 100 x 100 μm. Then by using the following equation we associated pressure changes with voltage. Then by using equation (2.3) we associated pressure changes with voltage. This equation was obtained from [36] by taking equations (11) and (14) and solving for voltage. We can then calculate the pressure difference, ΔP, across the tube from equations 3.3.6 and 3.4.1 for the steady

state flow and equations 4.6.1 and 5.5.1 from [16], we arrive at the following equations for

ΔP:

$$\Delta P_{steady\ state} = 4v_{max} * \mu * \frac{L^2}{a^2},$$  (2.4)

$$\Delta P_{puslatile\ flow} = \frac{v_{max} * \mu * \Omega^2 * L}{i * a^2 \left(1 - J_0\left(\frac{i-1}{\sqrt{2}} * \Omega\right)^{-1}\right)}$$  (2.5)

where $v_{max}$ is maximum velocity,  is blood viscosity, $L$ is the length of the stent, a is

radius of the artery, and  is the Womersley number. By assuming that the pressure drops

kL=σ, we can solve for expected voltage.

Results and Discussions:

Our results demonstrate that given a maximum blood velocity and assuming either

laminar or pulsatile flow, we can predict the voltage difference between the two cantilever

sensors in μV, a measurable value.

Figure 2-4.Stent Occlusion Diagnosis – Pulsatile Flow Assumption Data.

Demonstrating the resulting µV & Pa difference across cantilevers given different flow assumptions across three different conditions.

| Pulsatile Flow Assumption | | | |
|---|---|---|---|
| **Blood Flow Velocity Inputted** | **Output Type[Voltage/Pressure]** | **Diseased Patients** | **Healthy Patients** |
| *Minimum Blood Flow Velocity* | Voltage Difference [µV] | 112.45 | 56.23 |
| *Minimum Blood Flow Velocity* | Pressure Difference [Pa] | 3.61 | 1.81 |
| *Average Blood Flow Velocity* | Voltage Difference [µV] | 351.53 | 351.53 |
| *Average Blood Flow Velocity* | Pressure Difference [Pa] | 11.29 | 9.24 |
| *Maximum Blood Flow Velocity* | Voltage Difference [µV] | 915.54 | 894.74 |
| *Maximum Blood Flow Velocity* | Pressure Difference [Pa] | 29.41 | 28.74 |

Figure 2-5.Stent Occlusion Diagnosis – Laminar Flow Assumption Data.

Demonstrating the resulting µV & Pa difference across cantilevers given different flow assumptions across three different conditions.

| Laminar Flow Assumption | | | |
|---|---|---|---|
| **Blood Flow Velocity Inputted** | **Output Type[Voltage/Pressure]** | **Diseased Patients** | **Healthy Patients** |
| *Minimum Blood Flow Velocity* | Voltage Difference [µV] | 333.94 | 166.97 |
| *Minimum Blood Flow Velocity* | Pressure Difference [Pa] | 10.73 | 5.36 |
| *Average Blood Flow Velocity* | Voltage Difference [µV] | 744.03 | 608.75 |
| *Average Blood Flow Velocity* | Pressure Difference [Pa] | 23.90 | 19.55 |
| *Maximum Blood Flow Velocity* | Voltage Difference [µV] | 1625.36 | 1588.42 |
| *Maximum Blood Flow Velocity* | Pressure Difference [Pa] | 52.21 | 51.02 |

Conclusions:

Through our preliminary calculations, proposed a proof of concept for a piezoelectric dual cantilever pressure sensor to detect variations in blood flow patterns through a coronary artery stent.  Based on the calculations, changes in blood flow should produce a measurable voltage difference. Although voltage generation per cantilever was not measured, by assumption one of the cantilevers must be at least (for the healthy condition) 351 µV or 3.5 mV greater than its counterpart, thus even if the secondary cantilever produced no voltage, a 3.5 mV generation is still close to the 5 mV requirements

24

to keep the arguably more complex pacemaker sustained. Thus, by future work and iteration on the details on this design, a multiplicative of 10-20 cantilevers at this size theoretically may bolster a communication system for the blood flow sensor design.

2.3 Benchtop Studies

<u>Purpose:</u>

To further test the theoretical device, a large-scale pressure system was developed. The scale model was approximately 10x larger than the actual size and consisted of a series of PVC pipes with a 12V 6L/min peristaltic pump (to mimic the blood flow within the cardiovascular system). As seen below, two pressure sensors were attached the piping at the inlet and outlet with a .5ft distance between each of the sensors.



Figure 2-6.Benchtop Assembly for Stent Occlusion Diagnosis.

<u>Methods:</u>

In order to imitate the change in pressure in the artery, a ball valve was included to restrict fluid flow. The restrictions allow for changes in pressure which was recorded from the pressure sensors. As more of the valve was closed, the pressure difference increased as shown through the results in table 2-3. The amount of pressure varies depending on the cross-sectional area of the ball valve, giving elliptical closure rather than circumferential

closure. The difference in pressure proves that there is a pressure change when there is a change in area.
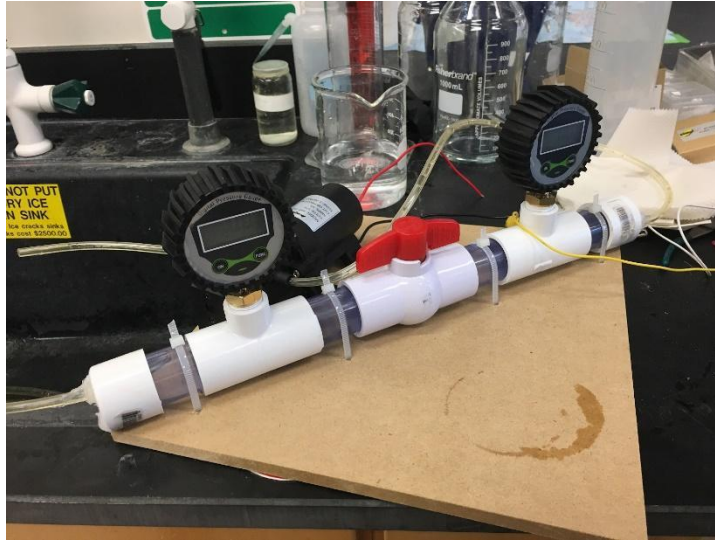


Figure 2-7. Benchtop Assembly for Stent Occlusion Diagnosis with Ball Valve

<u>Results:</u>

In the aftermath of the testing, the data showed that it was only until the ¾ closed condition did we see significant changes in the inlet/outlet results. A 75% blockage which is nearly the mount to which symptoms may start to be felt by patients, (approx. 70%). Although the results were unfavorable, that this is probably caused by the inaccurate sensors used or by the inaccurate test setup. Firstly, if the grade of the pressure sensors were increased it is likely that it would give a much higher accuracy beyond one decimal place. Secondly, by using a ball valve, it was difficult to position the valve at the multiple positions with precision. Thus, by a new setup explained more in the Future Work section, the hope is to increase these accuracy results as well as report the voltage generated expectations.

Figure 2-8. Benchtop Results for Stent Energy Harvesting Device.

Below are the results of the pressure difference between the inlet and outlet given differing cross-sectional area blockages.

.

| Trial Number | ΔP 100% (Pa) | ΔP 75% (Pa) | ΔP 50% (Pa) | ΔP 25% (Pa) 2 | ΔP 18.75% (Pa) | ΔP <18.75% (Pa) |
|---|---|---|---|---|---|---|
| 1 | 0.4 | 0.5 | 0.5 | 0.6 | 1.5 | 1.8 |
| 2 | 0.3 | 0.45 | 0.45 | 0.4 | 0.6 | 1.9 |
| 3 | 0.4 | 0.6 | 0.55 | 0.5 | 0.8 | 2.4 |
| 4 | 0.5 | 0.5 | 0.5 | 0.5 | 0.75 | 2.3 |
| 5 | 0.5 | 0.4 | 0.4 | 0.35 | 0.7 | 4.8 |

## 2.3 Intellectual Property

This idea first proposed in the spring of 2018, is currently under documentation review for patentability with the UCI patent office. A provisional patent is expected to be drafted and if the future work studies prove fruitful a full utility patent will be implemented.

## 2.4 Future Work

To build upon the prior bench study, this test bench will be created to replicate at a slightly higher accuracy the human artery. A 6 L/min peristaltic pump, with two pressure sensors, within a much small testing tube would be used. This tube, likely made of clear silicon, will be
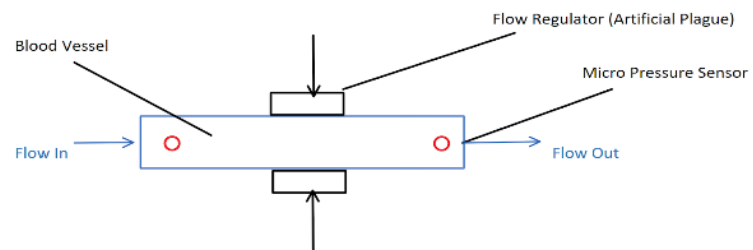


Figure 2-9. Schematic of the future flow test.

An artificial flow regulator will be implemented to compress on a 8-10 Fr size flexible tubing with micro pressure sensors installed at the inlet/outlet.

between 8-10 Fr, 3x the size of the needed structure and include a clamp two decrease the cross-sectional area in a more controlled manner.
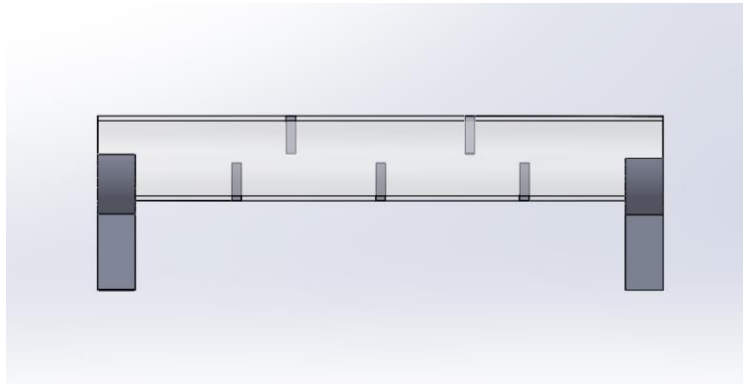


Figure 2-10. Solidworks Design of the future bench testing set up.

Featuring a compressible pipe outfitted with multiple pressure sensors at 30-60° offsets.

*Future Simulations:*

*Buckle and Squeezing Test*

<u>Purpose:</u>

In addition to the testing of pressure change, a test on the cantilever itself will be implemented to test the strength and flexibility of the material. The cantilever is comprised of primarily two materials: nitinol for its flexibility and polyvinylidene fluoride (PVDF) for its chemical resistant barrier coating. The cantilever is constructed using a nitinol wire which will be centered in the middle with the PVDF coating surrounding the wire. To test the strength of the



Figure 2-11. Schematic of the future buckle test.

The test will measure the maximum normal force a Nitinol/PVDF can withstand until fracture an important characteristic given the crimped use case it must undergo.

cantilever, a simulated buckle test will be implemented with a downward force equivalent to the

approximate forces faced during crimping of the stent. This test will push onto the tip of the
cantilever, bending the cantilever to see when it will begin to fail and break.

Methods:

To test for the piezoelectric generation upon the specific cantilevers COMSOL will be loaded
with load the approximate forces calculated via COMSOL from the initial blood flow velocity to see
the (1) the pressure difference across cantilevers and (2) to determine the voltage generation
possible for the energy harvesting application
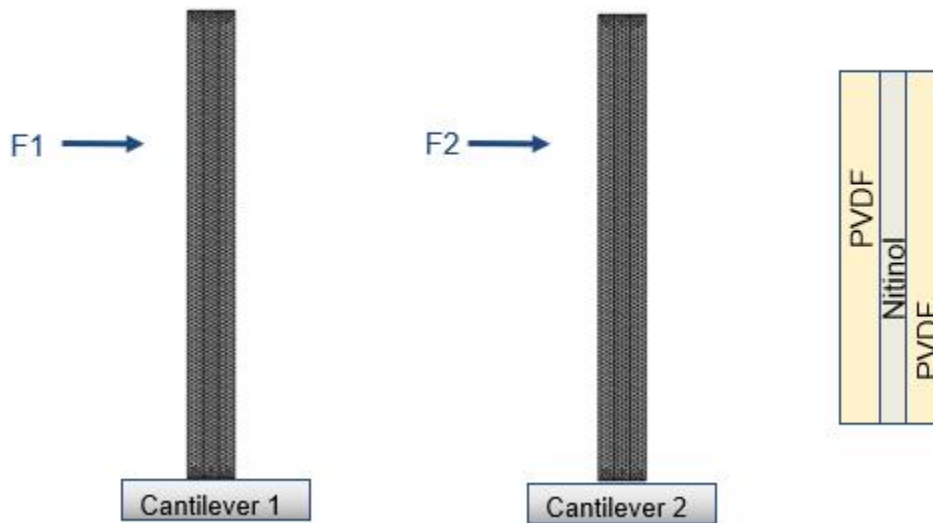


Figure 2-12 Future COMSOL simulation to measure the approximated voltage generation given
piezoelectric effect caused by deforming the Nitinol/PVDF cantilever.

## Chapter 3 - Energy Harvesting for In-Ventricle Pacemaker -Ferrofluid Design

3.1 Design Details and Iterations

This design may be summarized as converting previously wasted energy via friction or blood pressure onto the wall of leadless pacemaker devices into power to recharge the implantable device. To define the invention, there are three concepts: (1) electromagnetic induction, (2) blood flow in the heart, and (3) electrical recharging. Simply, the translation of a magnet across a magnetic coil produces electricity. A solid magnet has clearly been shown to provide such a voltage, yet in nature there exists an interesting magnetic fluid known as ferrofluids. These when localized between permanent magnets have the ability to become magnetized and thus act as a magnetic fluid. Such a fluid would then be compressible in nature and given a pressure would deform or move in correspondence to the pressure gradient. Thus, if an upward constricting pressure would be applied to a cylindrical container of such a fluid the net movement of the fluid would progress upward. Then, the movement of the magnetic fluid, inside of the electric coils would then begin to generate electricity, as noted by the electromagnetic induction theory in physics. To apply such a force, note the environment to which this device would be maintained, the heart. Oscillating between the filling and pumping stages, the hearts blood flow offers an excellent opportunity to demonstrate the forces required to make such an invention work. During the pumping stage of the heart, the blood within the ventricular cavity would be forced out to due to difference in pressure between the two chambers (ventricle and aorta). Uniquely the heart wrings out the blood within itself in the same motion as squeezing the water out of a wet towel, the motion that is desired to move the ferrofluid from rest up the cylindrical

container. At the filling stage of the heart, the blood would pool into the ventricle chamber decreasing the pressure onto the device and thus allowing the ferrofluid to return to a resting position. Upon generation of the electricity, the voltage would then be sent to a circuit where a large capacitor could store the energy and charge the pacemaker when needed. The form of such a device would be intended to have a soft outer wrapping to protect the blood from the ferrofluid, yet still allow for the deformation of the fluid. Within the wrapping would be the ferrofluid, a set of electronic coils, and a set of permanent magnets. Below is the initial design sketch of the proposed device.
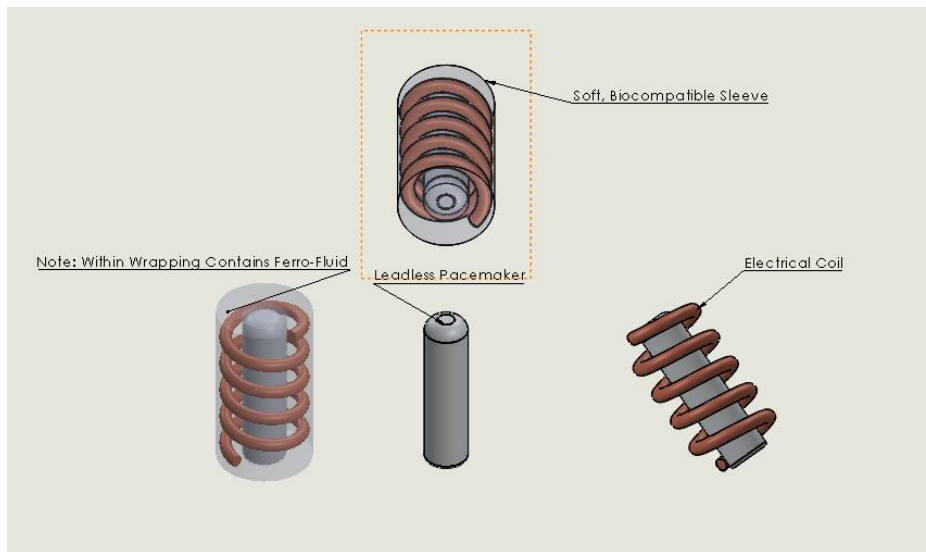


Figure 3-1.The Solidworks rendering of the ferrofluid energy harvester for in-ventricular pacemakers.

initially propose device which will encapsulate the leadless pacemaker with a soft biocompatible sleeve which when deformed will move the ferrofluid within and thus by electromagnetic induction create a voltage charge which may charge the leadless pacemaker.

## 3.2 Simulation Studies

Overview:

Two simulations were conducted upon the proposed device, focusing primarily on the compressible sleeve, and the potential induced voltage. The purpose of the

31

compressible sleeve study was to conclude if PDMS would be a valid material for the use of this device, specifically if the static pressure from the ventricle would be enough to displace the sleeve membrane and if the frequency of oscillation would cause potential modal defections.

*Compressible Sleeve Material.*

<u>Purpose:</u>

The Solidworks Simulation package assisted in the compressible sleeve optimization where the static load scenario was applied during the condition of systolic pressure in the left ventricle. The goal of this study was twofold -- (1) to determine if a significant deformation would occur given the pressure induced in the heart, and (2) if yielding would occur during the high-pressure moment.

<u>Methods:</u>

As can be seen below, both conditions were satisfied after the following parameters were implemented namely a fixture on the bottom face of the device (as this would be the implant surface), 140 mmHg, the average peak systole pressure, applied to the cylindrical exterior face. PDMS constants such as Young's modulus, Poisson's ratio was further implemented into the simulation design.

<u>Results:</u>

Results noted a max displacement of .3965 mm and max Stress 167 MPa. This displacement was significant considering the exterior thickness was assigned 2 mm by the current design an ~20% deflection. Further the stress was far below yielding point of 223 MPa, thus allowing for long term reliability of the device.
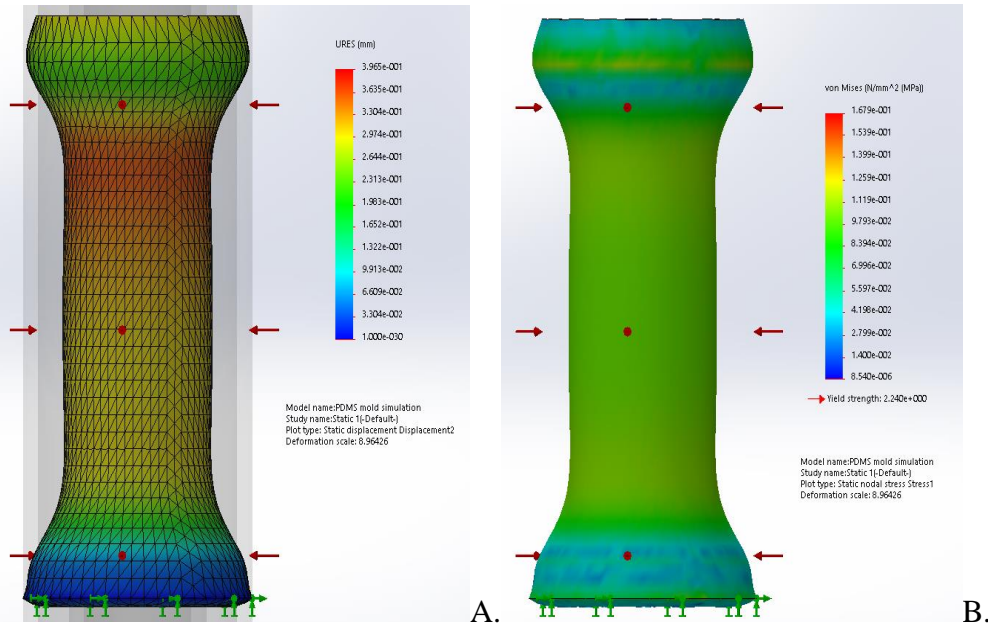


Figure 3-2. Static Simulation results on a PDMS sleeve.

Results from a 140mmHg pressure along the cylindrical face with a fixture along the bottom of the cylinder showing in A, a maximum displacement of .3965 mm and in B, a max stress of 167 MPa.

**Frequency Analysis.** A modal or frequency analysis was imperative for the definition of such an implantable device namely due to the oscillatory moment caused by the cardiac space would induce a strong resonating frequency between 1-3 Hz. Solidworks further provided a modal analysis package which this team used to analyze the device given a fixture condition on the bottom face. The material used was PDMS and the resulting resonance frequencies were determined to be inconsequential to the environment of this device as all modal frequencies were above the 1-3 Hz range namely greater than 4000 Hz. Thus, further proving the safety of the device.

A.


B.


C.


D.
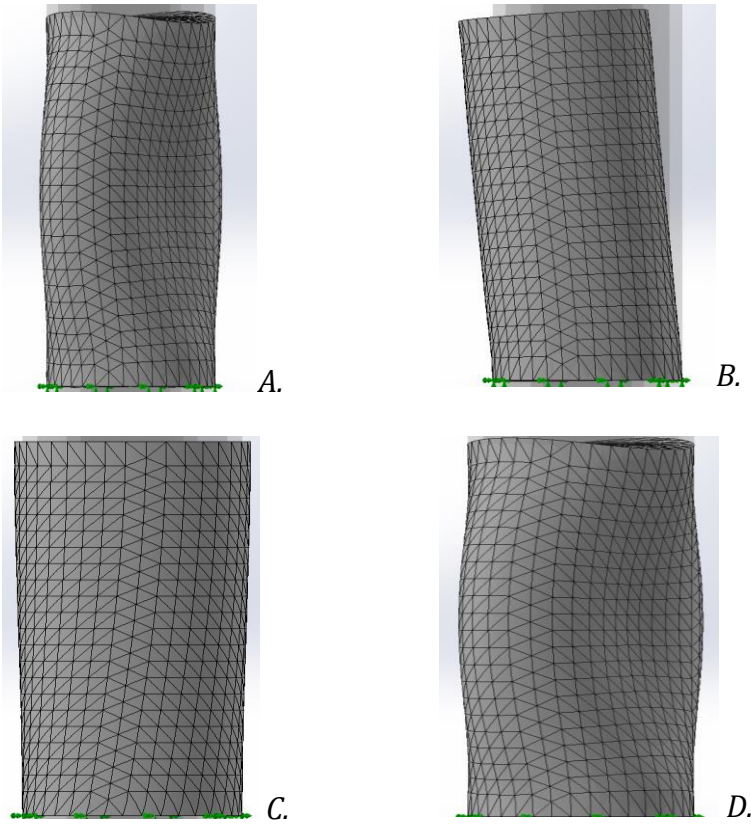
Figure 3-3. Modal Analysis Report

The table consists of the first five resonance frequencies all of which were noted to be over 4000 Hz.

| Mode No. | Frequency (Hz) |
|---|---|
| 1 | 4085.4 |
| 2 | 4087.5 |
| 3 | 7318.2 |
| 4 | 8210.9 |
| 5 | 8211.7 |

Figure 3-2. Ferrofluid Design Modal Analysis.

In A-D, the modal frequency outputs given a fixture on the bottom face and the use of the material PDMS. The resonance mode shapes re displayed in these graphs, however the analysis proved that

**Induced Voltage Analysis.**

Purpose:

      We investigate the induced voltages that were to be further proven in the bench top testing to determine potential power from the conceptual device. COMSOL, the multi-physics modeling software offered its sophisticated moving mesh conditions to allow a time dependent analysis of ferrofluid conditions.

Methods:

      In the ferro-fluid condition a 2D axis-symmetrical simplification was implemented given the symmetry of the problem i.e a cylindrical coil and a cylindrical ferrofluid compartment. The ferrofluid was modeled as a 1 inch tall within the ~¾ inner diameter inch cavity this assessment was given, due to the in-lab condition of using a test-tube filled with the fluid to ensure fluid movement during the experiment. Ferrofluid conditions were modeled after the EHF1 ferrofluid of 400 gauss strength used in the experimental study. Two magnetic caps, made of three N42 (2455.1 Gauss) and 3 N52 (3627.4 Gauss), were placed to provide a permanent magnetic field to stimulate the ferrofluid. The coil used was set to also demonstrate the experimental conditions, a 160 turn , 3/4" outer diameter and 1/2" inner diameter being 8.3 cm long with a 20 AWG wire size. Results are demonstrated below to show the integrity of the study and the possibility to simulate the experimental conditions. Notable is the ~4 mV output which correlates to the 6 mV, before 10x amplification, output of the experimental study.
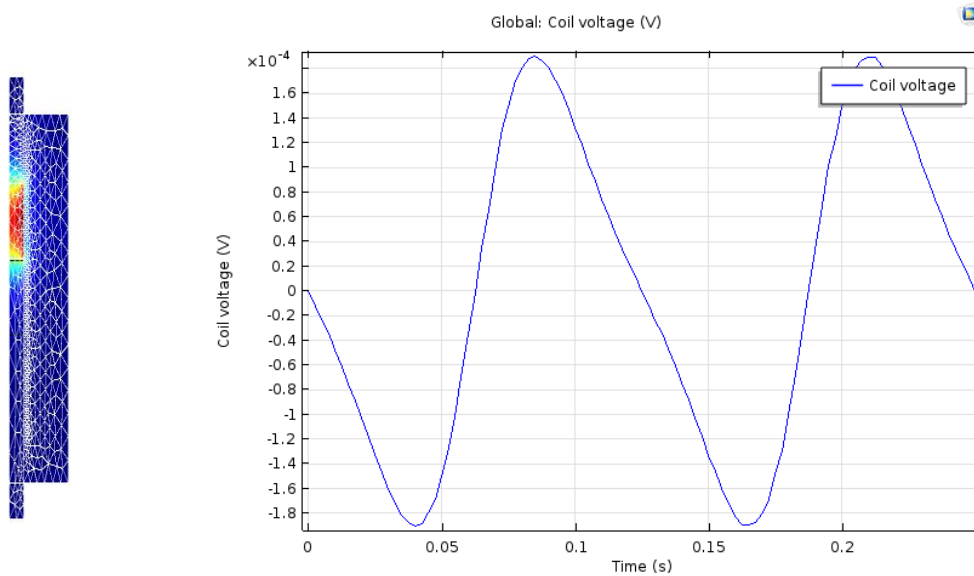
Figure 3-4. Ferrofluid Induced Voltage Simulation.

Where A shows the 2D axis-simplification set up in which the ferrofluid compartment (shown in red) oscillates in the center of the cylindrical coil. In B, the output determined from the study was ~4 mV which is approximately the value obtained during experimental studies, validating our initial finite element analysis methods, and allowing for future micro conditions to be applied.

Results:

The following table summarizes the simulation findings for induced voltage, where the solid core magnet would generate approximately 50mV in comparison to the 4mV created by the ferrofluid, which although significantly lower, would still reach 80% of the listed 5mV acceptance criteria given the larger test setup. However, this as will be noted in the next section was a cause for concern as the model now 3x scaled with an additional 10x scaling would thus prove far too weak for intended use.

Figure 3-5. Ferrofluid Induced Voltage Results.

These results are calculated from the ferrofluid and solid core magnet trials where a 3x scaling factor from the actual implant are recorded. Notably both simulations generated above the 5mV requirement during the 3x scaling but in the 1x scaling the ferrofluid failed its 5mV acceptance criteria.

| Magnet Type | Scaling | Voltage Output | Scaling | Voltage Output |
|-------------|---------|----------------|---------|----------------|
| Solid core  | 3x      | 50 mV          | 1x      | 16.6 mV        |
| Ferrofluid  | 3x      | 4 mV           | 1x      | 1.3 mV         |

## 3.3 Benchtop Testing

<u>Benchtop Testing Overview.</u>

Benchtop results have been completed using both (1) solid core and (2) ferrofluid to prove our devices feasibility. Initial macro-scale experiments conducted by the team with a solid core magnet and copper coils have served as proof-of-concept tests to induce electromagnetic fields and produce voltage.

*Solid Core Experiment.*

<u>Purpose:</u>

For foundational proof of concept tests, the team wanted to show the efficacy of the test set up by inducing an electromagnetic field using a solid magnetic core and a copper coil. Before the experiment was run, the team conducted a series of hand calculations and determined that the voltage that was expected to be output by the experiment was approximately 5 mV. The goal of the experiment was to prove that experimentally found values could match up with the theoretical values that were calculated.

Methods:

A simple robotic arm was constructed from the Aideepen, aluminum arm kit. Small 10 kg torque servos were used to actuate the arm. To control the robotic arm, an arduino code guided the desired range of movement and frequency. The robotic arm was used to grasp the magnetic core and oscillate it in and out of the copper coil. The coil the team used was a 160-turn outer diameter ¾", inner diameter ½", 8.3 cm long, 20 AWG wire with 6 small grade N52 Neodymium magnets. Through an initial dry test of the experiment, the team found that the magnetic strength of the magnetic core was insufficient to create any voltage when oscillated between the two ends of the copper coil. Two Arduino microcontrollers were used in the experiment; one was used to drive the servos in the arm, and one was used to read the output voltage. The second Arduino, working in tandem with a Matlab code was able to read the output voltage of the experiment and relay that data to the Matlab code, which plotted real time data that was being collected. The data that the team collected is shown in the figure below.
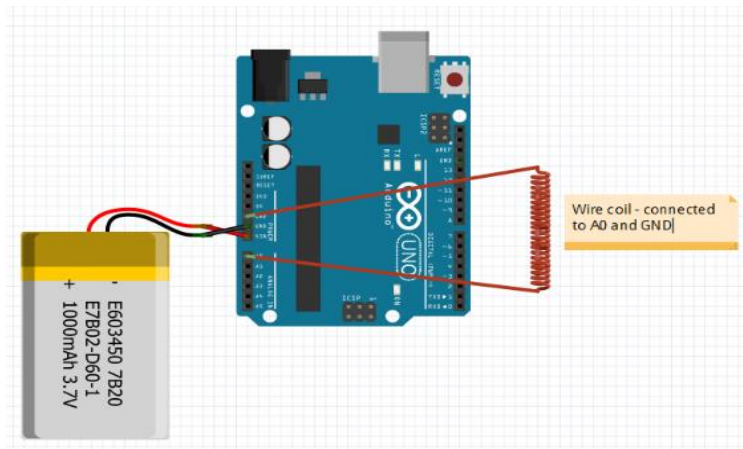
A.
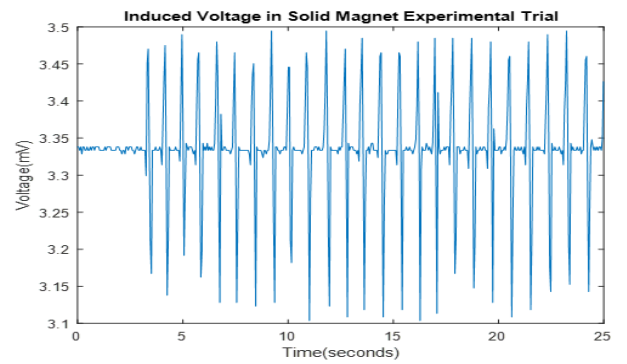


B



C

Figure 3-6. Benchtop Results for the Ferrofluid study.

In A, the circuit diagram for the solid core study, where a 3.35 input voltage from the Arduino acted as a baseline offset to allow for the data to be read in the Arduino (given that it may not read negative voltages), In B, the output from the study which shows maximal voltage differences to be ~60 mV. In C, shows the robotic arm used to ensure consistency during the study.

Results:

Experimental results yielded voltage outputs on the scale of close to 60 mV. This is more than the team expected a gain of 20%.


*Ferrofluid Experiment.*

Purpose**:**

Since ferrofluid has magnetic properties, our team tested electromagnetic induction and used the same experimental method by using ferrofluid and a copper coil.


Methods:

In continuation of the first experiment using the magnetic core, the same setup was used for the ferrofluid experiment. Instead of using the magnetic core, it was replaced with ferrofluid, filling the copper wire coil about half full with ferrofluid. To prevent leakage, the coil was plugged using PDMS with 3 N42 (2455.1 Gauss) and 3 N52 (3627.4 Gauss) neodymium magnets connected on both ends of the coil. The coil was then attached to the robotic arm which had an altered code to account for the weight of the overall coil. The robotic arm oscillated at a constant rate of 1Hz per second to mimic the frequency of the heart. Through this experiment, an Arduino was used to capture the output voltage generated from the ferrofluid and plot the data into Matlab.

Since the ferrofluid itself does not generate enough current within the copper wire coil, the decision of creating an amplifier was proposed. The circuit created was a non-inverting DC circuit with a 10x gain using an operational amplifier and 10k ohm and 100k

ohm resistor. An external power source was connected to the circuit, giving an input of approximately 10.15 V. Instead of collecting data through the Arduino and Matlab, these trials were captured through the oscilloscope and the software Analog Arts Instruments. Initially, the coil was attached to the robotic arm to be oscillated at 1Hz per second. Due to the limited range of motion of the robotic arm, the ferrofluid was unable to consistently move across the full distance of the coil. As a result, the ferrofluid was moved manually by hand at a rate of 1Hz per second.
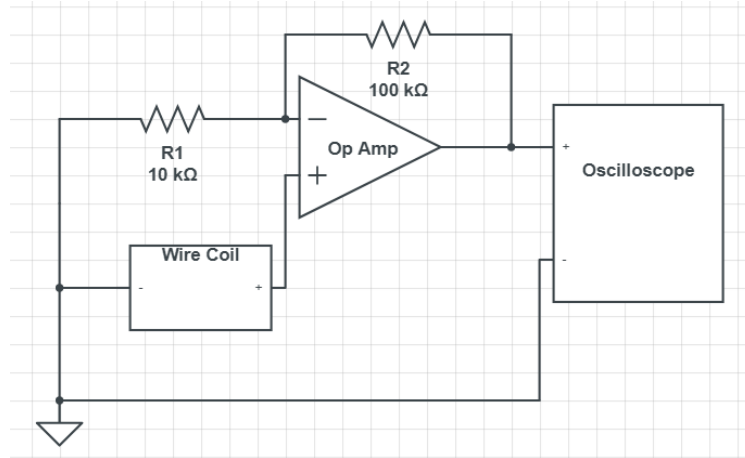


Figure 3-7.The Ferrofluid Circuit Benchtop Setup.

As seen in the circuit schematic (left), the experimental wire coil is attached to the positive input terminal of the operational amplifier. The 100k ohm and 10k ohm resistors are arranged to give the system a gain of 10, with the output being read by the oscilloscope. The operational amplifier is powered by an external source, not shown in the diagram, of +10V and -10V.

Methods:

In the initial experiment, there was an input of 3.35 V from the Arduino since the ferrofluid generated a miniscule amount of voltage. However, even with this addition input of voltage, the results showed that the ferrofluid either did not produce enough current to be collected or did not display any signs of movement. Because of the strong external

magnets, this may have caused the ferrofluid to stay at one end of the coil instead of

oscillating back and forth across the device. To account for this problem, an extra distance

was added between the bottom of the coil and the magnets. This adjustment allowed the

ferrofluid to oscillate across the device, however, there still was not enough current

generated to be seen. In order to capture the minimal current generated by the ferrofluid,

the coil was hooked up to an oscilloscope instead of the Arduino. Through the oscilloscope,

it captured some signals, but it was concluded that these signals were only reading the

noise from the wires or other external sounds. As shown in the data below, the voltage

produced was approximately 3.3 V which was the amount of voltage inputted by the

Arduino. There show no signs of voltage produced by the ferrofluid in the coil.
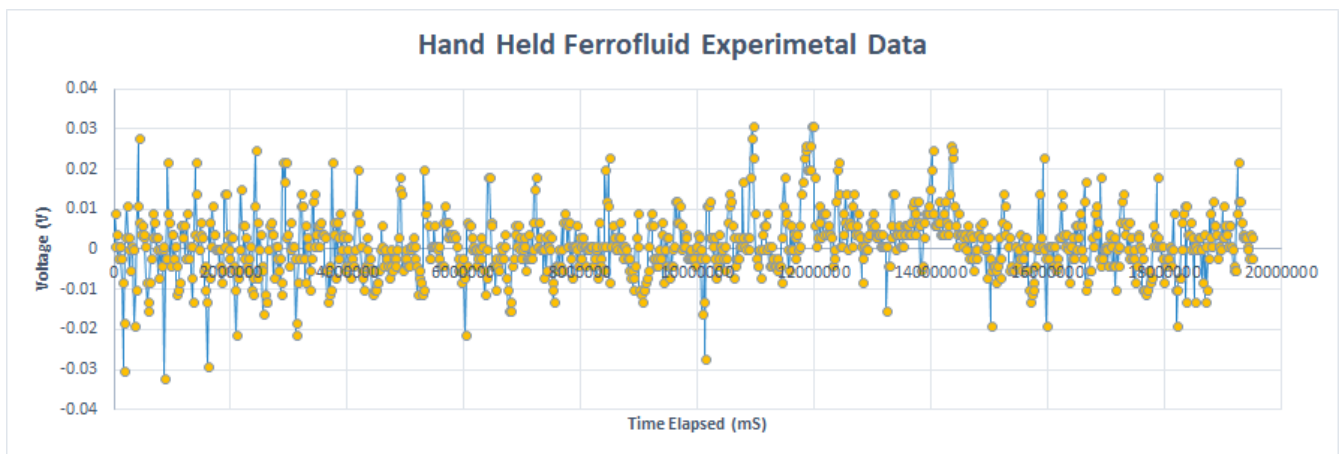


Figure 3-8. Ferrofluid Benchtop Results.

 The 10x amplified voltage is plotted as a function of time elapsed during the test. A relatively constant 30-60 mV reading
is shown on the plot. The actual voltage produced being on the scale of 3-6 mV.

With the addition of the amplifier, results were shown through the digital analog

oscilloscope. The amplifier of 10 gain yielded voltage outputs of about 60 mV which was

the expected voltage output calculated from the N52 and N42 magnets. These outcomes

display that there is current produced from the ferrofluid and it is not just capturing external noise from the wires. The data shown below depicts the amount of voltage produced over a certain amount of time from manually moving the ferrofluid across the coil.

Relating the collected data to the goal of producing 10 μW to power the pacemaker, we find that by using the collected 60 mV , 6mV (prior to amplification ), and 2mV (after 3x de-scaling), a known value of 500 ohm impedance for the Medtronic Micra Pacemaker[25], we use Ohm's law to find that this experiment produced approximately 2.4 μW of power, slightly under the 10 μW needed to power the modern pacemaker.


## 3.4 Intellectual Protection

Given the excitement that initially followed the benchtop series especially at the proximity the team was the 10 μW goal, the team filed with the UCI Patent Office in 2018 and obtained the provisional patent, listed as 62/673,784. However, in the winter of 2019, the team henceforth abandoned the research method and patent due to the technology's low capabilities in comparison to solid magnets. The concern is thus noted below.


## 3.5 Cause for Concern

There were three concerns which prompted the redesign of the energy harvesting strategy, (1) only on the 30x scale (10x gain factor and 3x physical scaling) yielded any applicable values for energy harvesting technique, (2) the benchtop data (with the 2.4 uW) was only produced during hand shaken (as the robotic arm failed to generate enough voltage) which likely produced more forces than are seen in by the blood pressure or

vibrational energy. (3) Even after three attempts of minor design changes such as increasing the ferromagnetic magnetism by increasing the density of the iron additives, altering the pump mechanism by shifting to a distal balloon instead of side vessels, adding mm magnet needles, and even using side permanent magnets the team failed to achieve result that initially captured the attention of the team.

Perhaps most key were the three following tests benchtop tests which were studied to characterize the ferromagnetic properties against solid core magnets. In the first experiment, we studied the effect of altering the pump mechanism by shifting the large diameter distal balloon that would contain a larger reservoir of ferrofluid in comparison to the cylindrical sleeve. We hoped that by increasing the volume of displaced ferrofluid and the velocity of the fluid we would see an increase in the voltage however, we ran a test where the ferrofluid was maintained similar to prior tests, (1) injected via a 1ml Syringe, (2) injected via a 20ml Syringe, (3) at rest (no movement of ferrofluid) , (4) and even with two moving side magnets all of which showed minimal increases to the baseline data of .01 <mV under no gain factor.
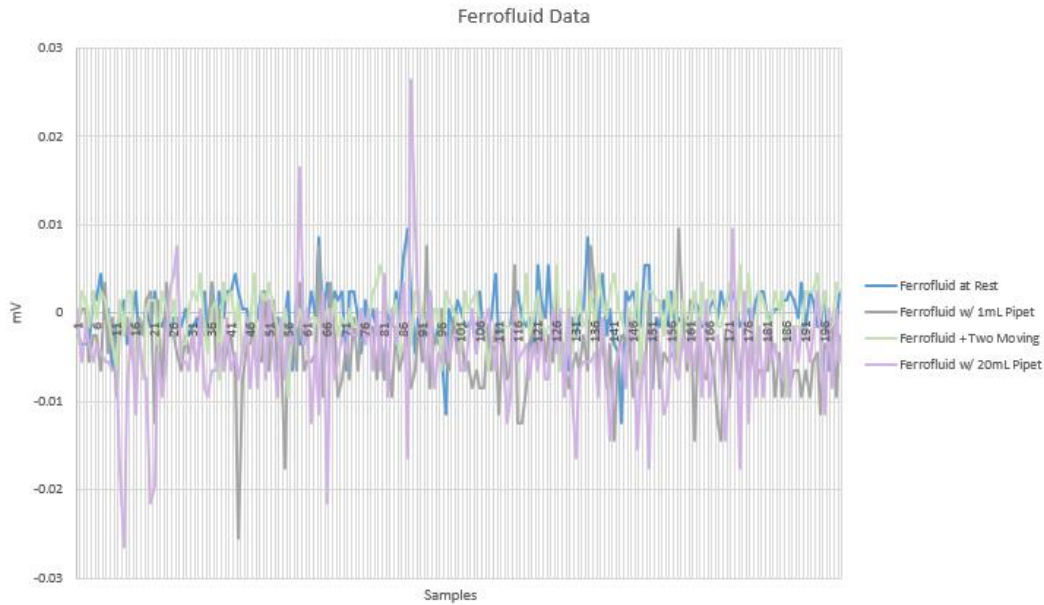
Figure 3-9. Ferrofluid with increased injection volume, the voltage output comparison.

Where four test conditions are shown, rest (control) where the ferrofluid was stagnant, with a 1mL pipet, with a 20ml Pipet, and with the incorporation of 2 side N52 neodymium magnets (a variable to see if increasing the magnetism would necessarily in the voltage output.

The second test we ran focused on the promise of the use of side magnets to add to the electromagnetic induction. The key question we wished to address, is whether having a moving magnet on the inside of the coil would produce equivalent voltage generation than side magnets or those located directly outside of the coils. Here we ran the following series of tests all of which contained no ferrofluid of (1) the rest or control where there were no magnets present to characterize the noise, (2) were we have the test case of two moving side magnets on either side of the apparatus, (3) one moving magnet, (4) one moving magnet with the addition of a magnet within the core, (5) two moving outside magnets with the addition of the same N52 magnet in the core. Here we see that by the simple addition of adding the same magnet to the core (one moving magnet + core condition) vs. the two moving magnets is drastically different. It underlined that what needed to change

45

with the potency of the magnet inside of the coils. If we return to the governing equations

of magnetism, we can remember that a magnet field drops off as $1/r^3$. differential that with

the thickness of even by a few mms that the coils have along with the trajectory of the side

magnets moving away and then closer to the seen below in the figure 3-8 [40].
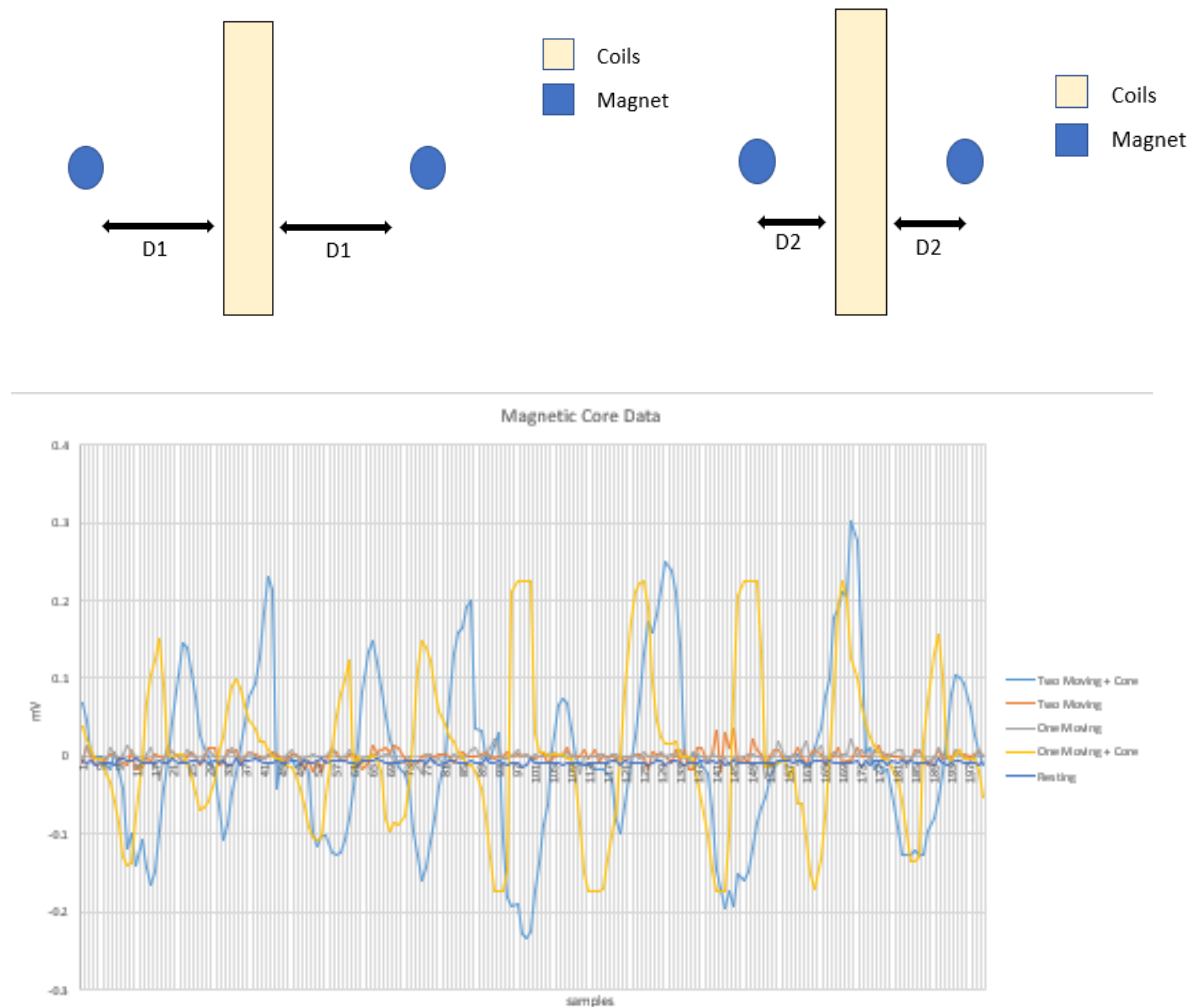


Figure 3-10. Inner vs. Outer Magnet comparisons.

Where the test set up is shown in (A/B) that two side magnets were set so that they would oscillate horizontally outside of the coils. The test conditions then followed with a rest (no moving magnets) condition, then variably adjusting the number of moving magnets in the inside/outside of the coils (C).

46

Perhaps most conclusively, is when we compare the ferrofluid condition with two side magnets against the core with the two side magnets, where the mV gain by the core is notably higher and with this last set of data, the team would require a new redesign by instead of looking at ferrofluid, we searching for a novel use of a solid core magnet.
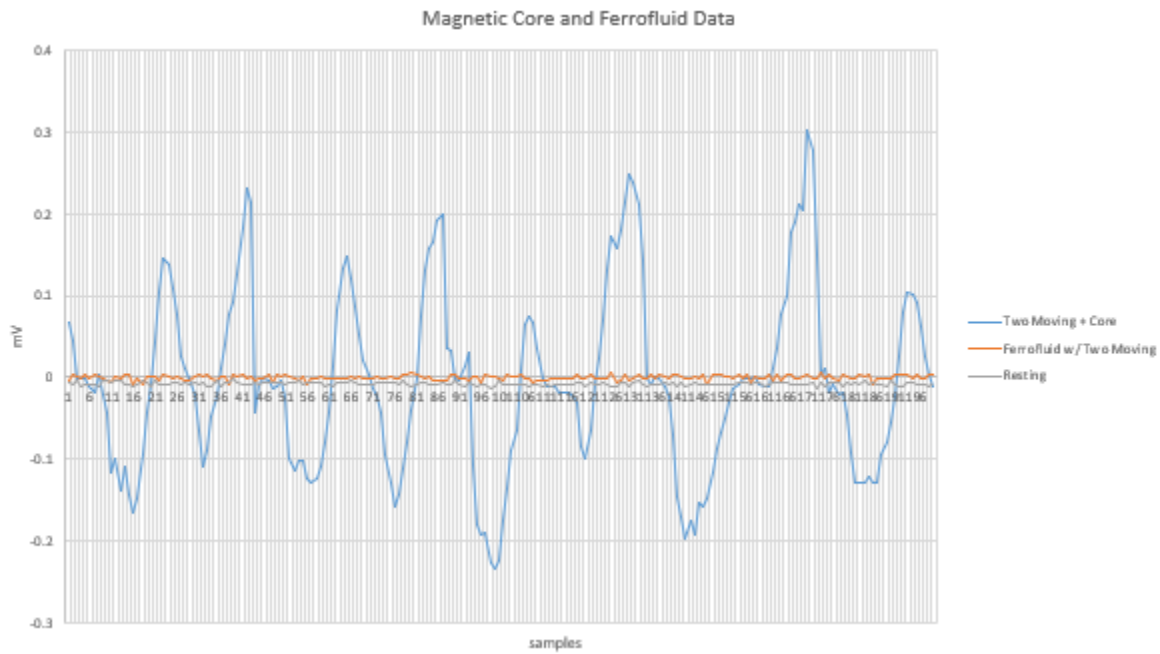


Figure 3-11. Solid Magnet vs. Ferrofluid Comparison test.

Where solid magnets in their best condition noted, with two side magnets and an inner core (a potential design considered) were used against the ferrofluid with two moving exterior magnet. The results clearly show that solid magnets outperform the ferrofluid condition, which prompted the design change described in the later chapters.

# Chapter 4 - Energy Harvesting for In-Ventricle Pacemaker: Magnetic Core

4.1 Initial Iterations A: Pump Design

After the conclusive results shown at the end of Chapter 3, a solid magnet triumphed over its viscous counterpart. Initially, the inner ferrofluid vessel was swapped with a solid core that would be displaced via the compression of a saline filled sack. By the use of hydraulics, the large pressure displacements in the heart were intended for a simple design. The transposed water would press against the solid magnet and by two-way check valves on the outer rim of the inside vessel the water could circle through the system. Thus, during high pressure cycles, the outer balloon would compress, forcing saline into the main compartment and then by translation, the saline from the secondary compartment would release into the first chamber. During low pressure events, the cycle would undo itself restoring the lost fluid into the secondary chamber as the pressure released off the outer balloon via overcoming the slight resistance from the two-way valve seal. To help describe the design, see the schematic shown below.

However, after feasibility testing on the device it was quickly found that (1) an 80% compression, the idealistic rate of the device would be improbable to overcome the forces in a tight system (see below of original test set up). (2) The creation of theses 1-2 mm diameter two-way valves would prove difficult during manufacturing due to the meniscal nature of the device. (3) Lastly, the design lacked a clear unstable equilibrium to which the magnet may rebound against.
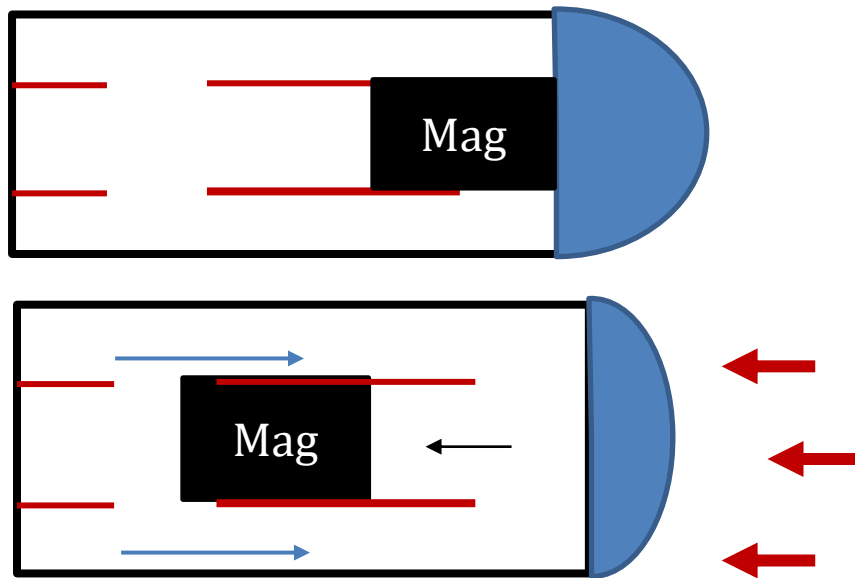
Figure 4-1.The preliminary prototype design of a solid magnet interface.

Where in (A) the relaxed state the magnet would not allow for the saline (blue) to penetrate behind the lined wall. After compression (B) the magnet pulses forward and the restoring force would be the hydraulic pressure the magnet must overcome in the contained space.

The team underwent the following three prototypes/ideals for the system all focused on establishing this unstable equilibrium for the solid magnet to rebound against the ideas included (1) a mechanical translation inspired by a camshaft/piston (2) displacement via a bottom and top diaphragm of saline, (3) compressive springs that would re-initiate after the top-diaphragms collapsing system, (4) lastly side magnets ideally compressed by the heart wall or blood pressure. In turn these designs did not reach succession due to (1) the high fatigue or stress points created at the joints between wheel and piston. As on such a small device (only 10mm thick) would leave room a fractional amount of space for an optimum piston system. (2) The system would have a constant pressure throughout the device, thus both top and bottom diaphragms would collapse displacing the magnet minimally. (3) held the most idealistic case, however if we return to the data, side magnets

in comparison central axis magnets pale in comparison to the electrical current generated,

which promoted the use of the following umbrella design.
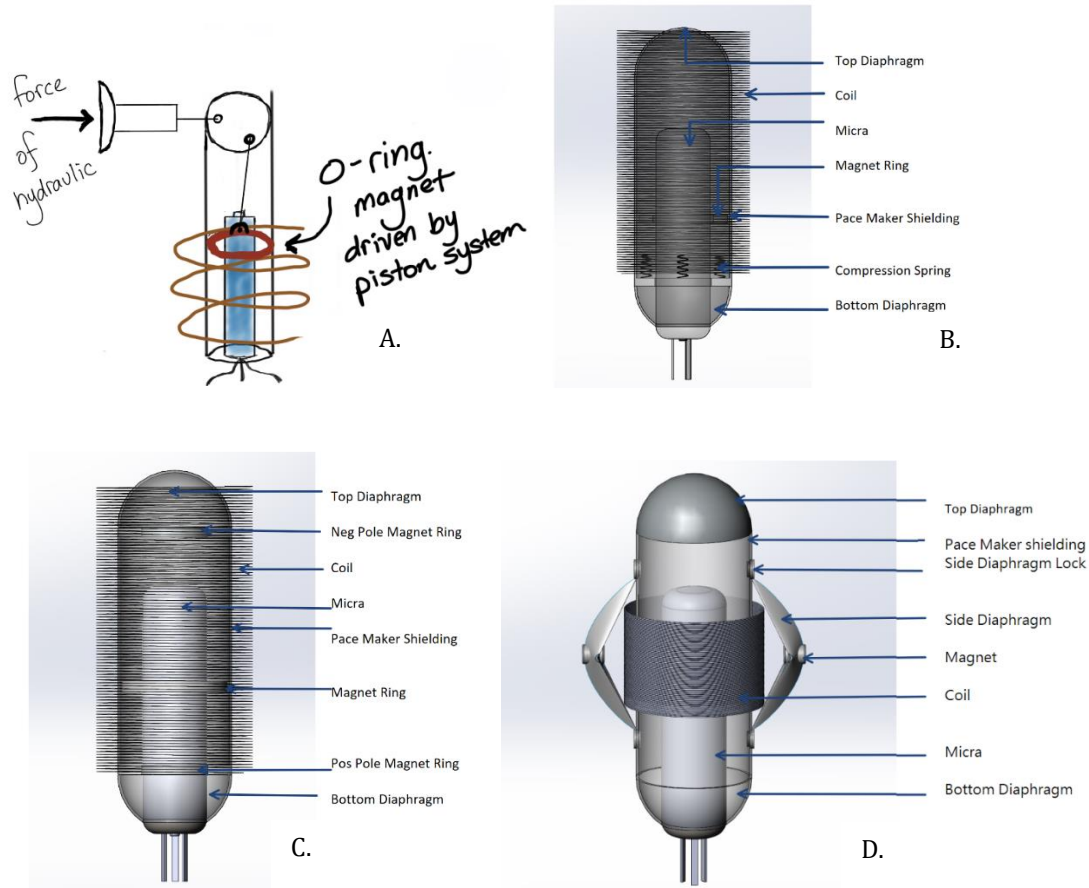


Figure 4-2. The four iterations of the initial Solid Magnet design.

The four designs consist of (A) Cam/Piston design, (B) Top and bottom diaphragms, (C) a compressible spring, (D) side magnets.

## 4.2 Initial Iteration B: Umbrella Design

As a progression from the above, the team proposed a secondary iteration based upon the umbrella structure to convert the contractile motions of the heart into linear motion. When the heart walls press on the umbrella arms, the center fixture is restricted to the path of the



Figure 4-3. Magnet Rider(Runner) movement during umbrella extension and compression spring.

vertical shaft, much like the rider in an umbrella design. This linear motion may now move magnets that will surround induction coils.

Overall, the new design may be visualized in rings of concentricity, in the first ring, a hollow core to be occupied by the Micra pacemaker or other in-heart pacemakers. Secondly, there is an inner cylindrical magnet with a Teflon jacket which loosely fits around Micra (with a 2 mm tolerance) to minimize frictional wear and to maximize the electrical generation. Since a magnetic field drops off in its potency as $1/r^3$, by decreasing the



distance from the central axis, the region of highest conversion, maximal electrical production may be achieved.
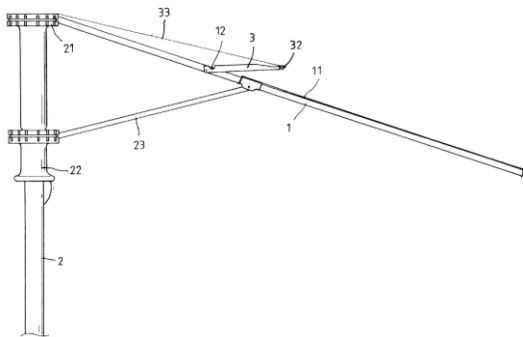
Figure 4-4. Side view of umbrella mechanical design.

Following this is a plastic which has the windings of the multi-turn coil used to transfer the moving magnetic field into an electrical current. Then, a thin 1.5mm PDMS coating is used to shield the coils and the inside body compartment from the outer environment. Lastly, the outer magnet is attached to the rider mechanism which traverses the longitudinal axis of the pacemaker from the linear conversion of the heart wall palpitations. The umbrella arms will be made of a lightweight material that has some flexible properties. It is imperative that the arms be made of a material that is highly resistant to the corrosive nature of the human body. The geometry of the arms must also be designed in a way that is easy to deploy with a catheter. They must be able to withstand millions of cycles of the heart walls rubbing on the surfaces as well.
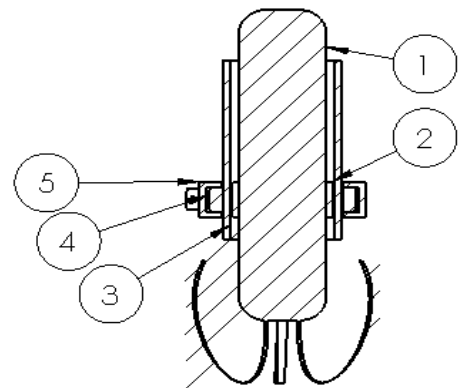


SECTION A-A

Figure 4-5. Cross sectional view of the umbrella assembly.

This view shows the inner magnet, coils, outer magnet, and primary rider attachment

| ITEM NO. | PART NUMBER | QTY. |
|---|---|---|
| 1 | Micra | 1 |
| 2 | Inner Magnet | 1 |
| 3 | Simplified Coils | 1 |
| 4 | Outermagnet | 1 |
| 5 | Rider | 1 |
| 6 | Strut | 4 |
| 7 | OuterStrut | 4 |
| 8 | Leaflet | 4 |
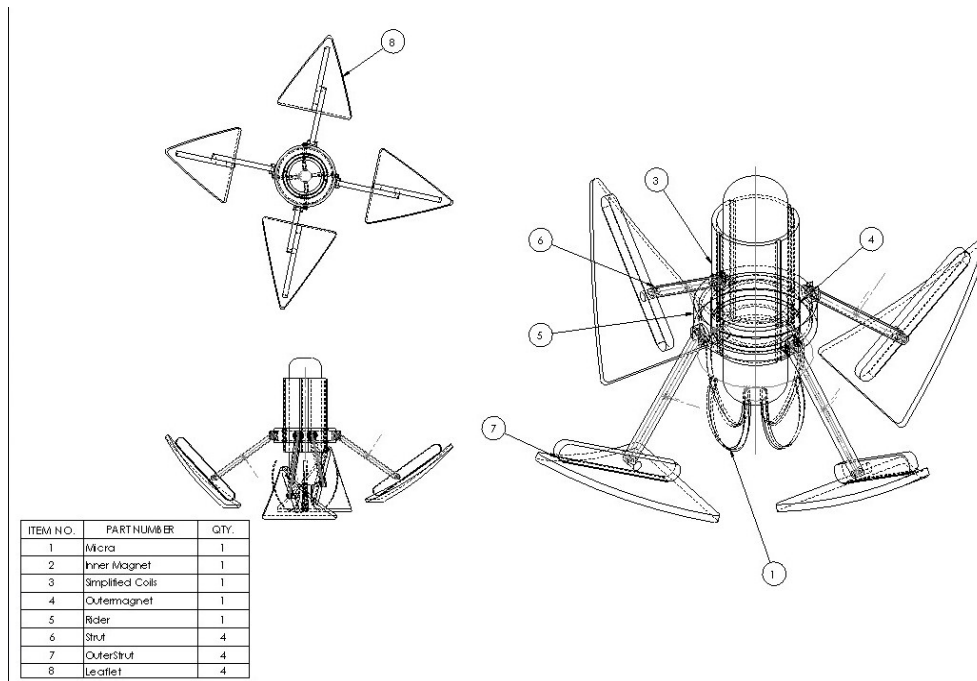
Figure 4-6. The assembly drawing of the umbrella design.

Where the Micra pacemaker encapsulated by the electrical coils, double magnet design, and the "Umbrella Design" noted by four splined soft plastic ridges that are mated to the

The primary downfall to this design is the necessary hinges. From prior research documenting the failure of early transcatheter heart valves, it was apparent that their primary failure points tended to be located at the joints specifically by blood clotting initiated at the hinge points [41]. Thus, the team required one final redesign that incorporated a single stent sleeve, which minimized the number of failure points via hinges, yet still incorporated the contractile motion powered by the side wall.

## 4.3 Final Iteration C.: Stent Design

Finally, the last iteration of the design was inspired after seeing the nitinol stent designs used by Medtronic for their trans-catheter aortic valve replacement (TAVR) designs. The porosity of the final stent design, with its cuts/struts lead to both an increased

elasticity and capability to elongate upon its primary axis. Furthermore, the nitinol material is well-cited as an FDA approved material noted in both TAVR valves and cardiovascular stents [42]. Below is an outline of the two modes of the device in its relaxed or "chubby" state and ¾ of its compressed state. With the movement of the distal lip of the stent, a ring magnet would be affected that would generate voltage by its moving current. A major design hurdle tackled is that magnets generated greater voltage by being placed coaxially within the coils. As such, an outer ring would be installed so that it would couple magnetically with an inner ring magnet. Viewing the design cross-sectionally, first would be an outer ring magnet, the coil sheath (made of PDMS material), coils, inner ring magnet, and lastly the pacemaker itself. On a related note, the potential for the inner ring magnet to rub and cause frictional wear against the inner pacemaker was a concern. Thus, a Teflon sleeve was added, as Teflon has one of the lowest coefficients of frictions for plastics at .04 [43]. For the outer design of the stent the team contemplated multiple versions of potential final design. These included differing size struts, from triangles, to diamonds, to serpentine cuts. Upon literature review, one doctoral student [44], discovered via FEA that diamond cuts provided the greatest structural rigidity between any other design and thus with the target of reaching near 10 years or about [44] cycles the team finalized a small diamond cut design for its longevity and for its elongation potential (smaller cuts).

1. Micra
2. Copper Coil Sleeve
3. Outer Ring Magnet
4. Inner Ring Magnet
5. Top Cap with Sleeve
6. Stent
7. Top &Bottom Stent Base
8. Bottom Cap
9. Inner Magnet Holder

1. Micra
2. Copper Coil Sleeve
3. Outer Ring Magnet
4. Inner Ring Magnet
5. Top Cap with Sleeve
6. Stent
7. Top &Bottom Stent Base
8. Bottom Cap
9. Inner Magnet Holder
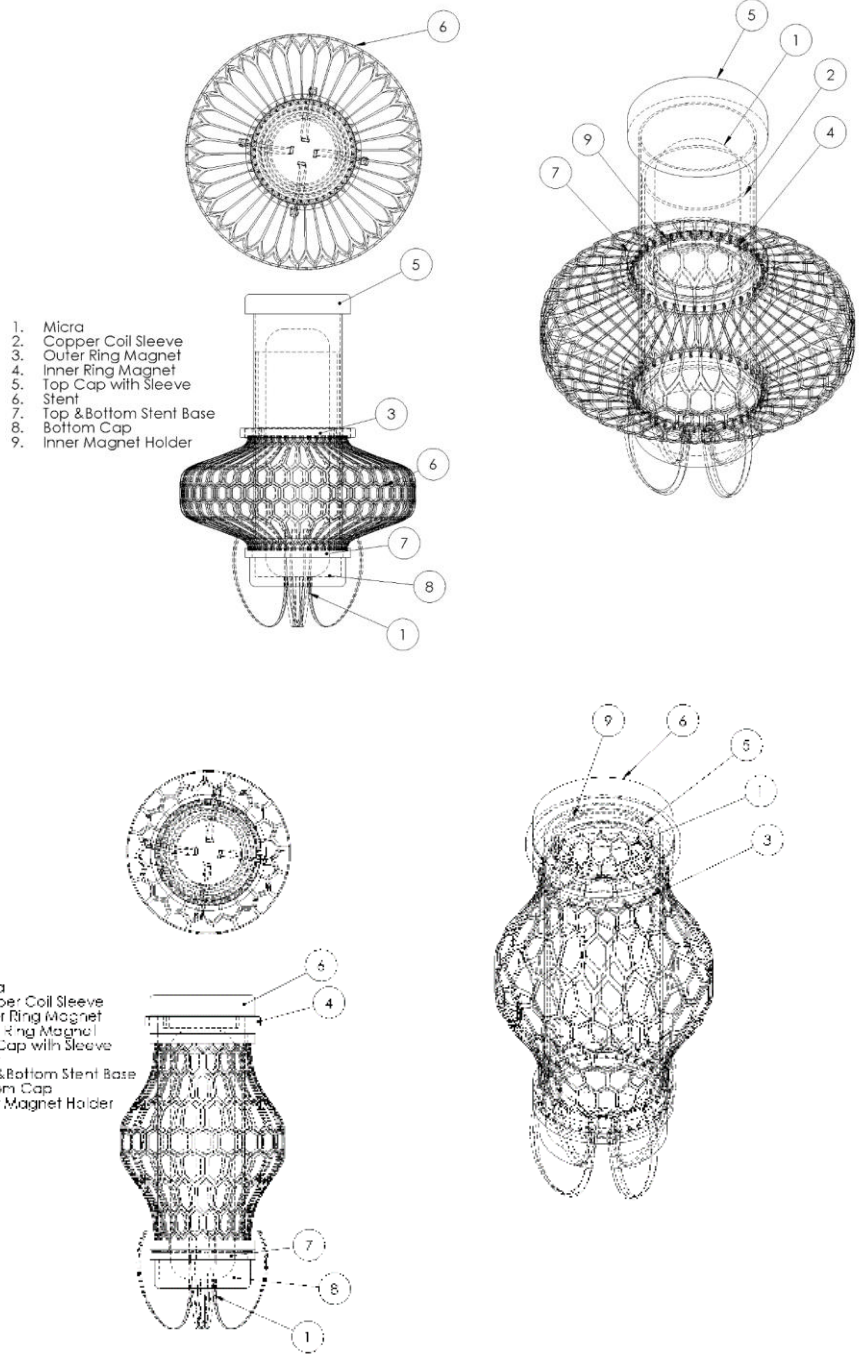
Figure 4-7. Final Rechargeable Pacemaker Design.
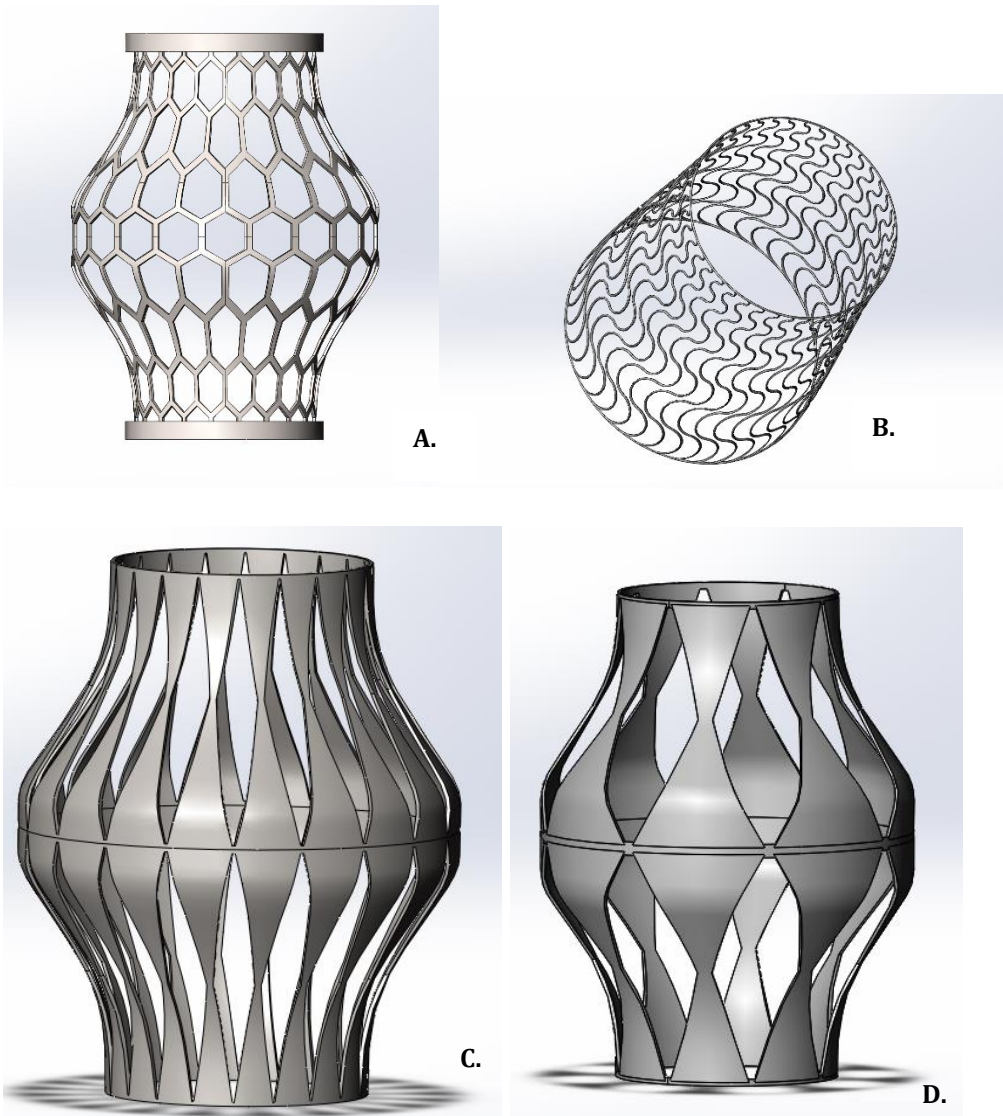
Figure 4-8. The Four Stent Design Considered.

Where B/C/D were considered but ultimately not chosen as they would lack the structural integrity of the diamond cut pattern.

## 4.4 Engineering Acceptance Criteria and Tests

To comprehensively test the finalized design the following table was created for the acceptance criteria and test description to prove the devices feasibility. By categories, we have (1) Modal Analysis (Simulation), (2) Induced Voltage (Simulation/Benchtop), (4) Heat Generation (Simulation/Benchtop), (5) Magnetic Shielding (Benchtop), (6) Mesh

Compliance (Simulation). These tests are outlined below in table 4-1 and serve as the basis

of all the test methods to be explored in the following chapters.

Table 4-1. Lists the experiments conducted for the stent designed energy harvester for in-ventricular pacemakers.

| Test Name | Acceptance Criteria | Test Description |
| --- | --- | --- |
| Induced Voltage (Simulation) | 10 µW or greater shall be generated by test set up. | Using COMSOL, the inner/magnet set up shall be tested for optimal electrical generation using the approved dimensions and 1x scaling. |
| Thermal Analysis (Simulation) | Surface temp shall not exceed 40 Degrees Celsius | Using COMSOL, the energy harvesting mechanism shall be inspected for heat generation from the current produced during actuation. |
| Mesh Compliance (Simulation) | Mesh shall deform 10mm given 100% of heart force | Using, COMSOL, the outer "stent" or mesh will have approximate heart force conditions applied radially along its outer edge, where the elongation of the tip of the stent shall be measured. |
| Modal Analysis of Pacemaker Design (Simulation) | 1-2Hz shall not be found as a fundamental frequency | Using Solidworks, a modal analysis shall be conducted to analyze the fundamental frequency of using the uniquely formed "stent". |
| Induced Voltage (Benchtop) | 10 µW or greater shall be generated by test set up. | Via a linear actuator, a simple inner and outer magnet set up shall be actuated where, the inner magnet slides inside the inner diameter of the 3D printed "Coils" guided by the outer magnet, being displaced by the linear actuator. |
| Magnet Shielding (Benchtop I) | Magnetic field shall be deflected greater than or equal to 75% from original field. | A thin, 1mm thick copper sheet, shall be inserted between the space where the Micra would be located, and the inner magnet. Both the inner and outer magnet shall be present, and the gauss shall be recorded using a gauss meter. |
| Magnet Shielding (Benchtop II) | Magnetic field shall be deflected greater than or equal to 90% from original field. | A thin, 1mm thick copper, nickel, mu-metal sheet, shall be inserted between the space where the Micra would be located, and the inner magnet. Both the inner and outer magnet shall be present, and the gauss shall be recorded using a gauss meter. |
| Magnet- Pull force (Theoretical) | Magnets do not separate during testing with lb force 3 times the heart | Using a theoretical analysis, the momentum of travel from actuation from the heart walls to the relaxation of the pressure shall be calculated using elementary momentum equations |
| Animal "Study" (Benchtop) | All parts fit within animal components | From a harvested pig heart, the 1x,2x scale devices shall be inserted in a cross sectionally dissected heart. |
| Thermal Analysis (Benchtop) | Surface temperature does not exceed a change of 2C | With the optimal PDMS thickness chosen in the above testing, the device shall again be manually actuated for 15 minutes and during which the temperature shall be recorded with and without active 6L/min water cooling |

# Chapter 5 - Magnetic Core: Simulations

5.1 Introduction to Simulation Methods

<u>Purpose:</u>

To begin the simulations, the force parameters caused by the heart wall onto the mesh or stent walls would need to be defined.

<u>Acceptance Criteria:</u>

As this is literature research would be primarily for data collection the acceptance criteria for the ventricular force would be set as a range, between 10N (the lowest feasible amount for the heart) and 1kN a value that would exceed expectations for such a pump.

<u>Abstract:</u>

As the pressure, defined as force/area, is well known within the cardiovascular system (167 mmHg -170 mmHg during systole and 10-11 mmHg during diastole left ventricle it is possible to  extrapolate the force provided from a surface area of the heart, near the apex where the device would be implanted. To find the apex surface area, two literature sources were examined for their surface areas during and after contraction. Then these surface areas were averaged between the two sources. Using the aggregating pressures and surface areas, force was calculated. Left ventricle systolic and diastolic force are 18.9 N and 309 N, respectively. Both values pass the acceptance criteria. To note, the team decided to focus on the left ventricle as its average pressure would greatly exceed the right and would be the best-case scenario for an implant.

<u>Background:</u>

The force was calculated from pressure and surface area using the relationship:

$$P = FA \qquad\qquad (5.1)$$

Which then may be re-arranged to:

$$F = A/P \qquad\qquad (5.2)$$

Knowing that  A is the surface area, P the pressure in the system, and F the cross sectional force the ventricular force for our simulations may then be calculated.

<u>Materials:</u>

Data was research in journals found using databases such as Google Scholar, PubMed, and EBSCO Academic Search Complete [45-51].

<u>Methods:</u>

Pressure values of swine heart ventricles were extracted from five sources. They were then compiled and separated based on whether the pressure was measured in the left or the right ventricle or whether pressure is systolic and diastolic. Whenever sources contained values for the pressure of the same categories, those data points were averaged. Data points from Source 1 were thrown out from the study because the pressures were taken after a pulmonary artery banding procedure. Total surface area of swine left ventricles were calculated by dividing scar area by the scar area percentages of left ventricles. The calculations determined from data from two different papers were averaged to be used for force calculations based on the pressure. Only the pressures of the left

ventricles were calculated because only the surface area data of the left ventricle could be found.

Results:

Table 5-1. Scar area and percentage and calculated total left ventricle surface area [41-47].

| Source (Paper Number) | Total LV surface area (m$^2$) | Average LV Surface Area (m$^2$): |
|---|---|---|
| 7 | 0.0163 | 0.0137 |
| 8 | 0.0112 | |

Table 5-2. Pressure of left and right ventricles during diastolic and systolic pressure and force of left ventricle[41-47].

| | Source 2 | Source 3 | Source 4 | Source 5 | Average (mmHg) | Average (pascal) | Force (N) | Pass/Fail |
|---|---|---|---|---|---|---|---|---|
| Left diastolic pressure (mmHg) | 11 | N/A | N/A | 10 | 10.3 | 1380 | 18.9 | Pass |
| Left ventricular peak systolic pressure | 167 | N/A | N/A | N/A | 169 | 22500 | 309 | Pass |
| Right systolic pressure (mmHg) | N/A | 30 | 27 | N/A | 28.5 | 3800 | N/A | N/A |
| Right diastolic pressure (mmHg) | N/A | N/A | 4 | N/A | 4 | 533 | N/A | N/A |
| Mean right ventricular pressure (mmHg) | 25 | N/A | N/A | N/A | 23.5 | 3130 | N/A | N/A |

Conclusion:

Although this is a crude measurement technique for ventricular force, due to the lack of data regarding the ventricular wall force, this rough estimate proved useful for benchtop testing/simulation studies. Finding literature on the ventricular surface area for the right ventricular were scarce and thus the ventricular wall force was not calculated.  However, examining the larger left ventricular pressure system does offer the benefit of a best-case condition as the this would directly translate to increases in the voltage potentially possible. Therefore, if from the data shown below, if we assume the structures are the same size, the right ventricle scales at approximately 3/20th of the force of the left ventricle.

5.2 Induced Voltage Analysis

Purpose:

The aspect of the device being simulated is the voltage output of the moving magnet inside the coil. Voltage output indicates how much power the device can generate for without enough generation of power, the pacemaker cannot sustain itself.  Specifically, analyzed are the number of coil turns, length, and thickness to find the optimized values as well as the feasibility for this device.

Acceptance Criteria:

The acceptance criteria for this study was set to the meeting the generation of 10 μW or 5 mV given a 500 (Ω) impedance.

Abstract:

The study was performed using COMSOL to model the voltage output generated from a moving magnet inside the coil. The dimensions of the device were incorporated into the study. A magnet displacement of 10 mm was found to yield the highest voltage output and a wire thickness of 30 AWG seemed to output the most voltage, with the exception of the 200 turn coil, in which the 34 AWG wire yielded the highest output. All in all, with 100 mA or more of current, the simulation suggests that the device provides enough voltage to pass the 10 µW acceptance criteria.

Background:

According to Faraday's Law, whenever there is a change in magnetic flux with respect to a coil with flowing current, voltage is generated, Faraday's Law:

$$\varepsilon = -N\, \Delta\phi/\Delta t \tag{5.1}$$

Where ε is the voltage, N is the number of turns, B is the magnetic field, A is the area, t is time. This study targeted altering the number of coil turns, as well as the area or gauge of the wire to optimize the necessary wire type to find the optimal 10uW production.

Materials:

COMSOL Multiphysics 5.4 including the Magnetic Fields and Moving Mesh packages were utilized.

<u>Methods:</u>

The simulation was conducted similarly to the Induced Voltage Tutorial provided by COMSOL. The geometric modifications added were the addition of the Micra and the dimensions of the margent and coil. The Micra width and height are 3.5 mm and 25 mm, respectively. The magnet width and height are 0.25 mm and 2 mm, respectively. The coil width and height are 0.25 mm and 20 mm, respectively. The temperature of the system was changed from the default 293.15 K to body temperature, 310 K. The remnant flux density was adjusted to be 1.32 T in the z direction. The prescribed mesh displacement (in the z direction) was changed to 10 mm. The coil turns were tested with 100, 200, and 300 turns and the coil width were tested with 24, 30, and 34 AWG. Lastly, the simulation was run with 10 mA of current with a 200 turn and 24 AWG coil.
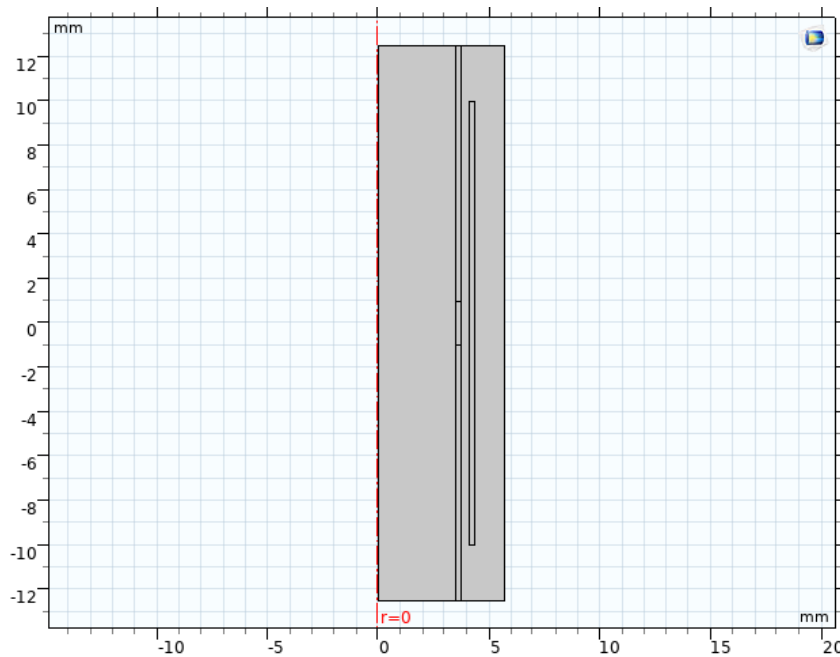
Figure 5-1. Induced voltage simulation geometric set up of the device, modeled on COMSOL 5.4.

Results:

Theoretically, the displacement of the magnet should be 9 mm as the magnet is 2 mm and coil is 20 mm and they are both centered at 0 mm. However, after testing with different values ranging from 8 mm to 11 mm displacement, 10 mm displacement was empirically found to generate the most voltage.

As expected from the Faraday's Law equation, as the number of coils increased, the voltage increased as well. The 30 AWG wire yielded the highest voltage for 100 and 300 turns, 1.614 mV and 4.812 mV, respectively. The 32 AWG wire yielded the highest voltage for 200 turns of 3.227 mV. For all wire thicknesses and number of coil turns, 1 mA is insufficient current to generate 10 µW of power, however a 10mA generation was more than sufficient for the task. A final test to determine the power generated from COMSOL was performed on a 200 turn and 24 AWG coil using 10 mA of current. The power generated was 30.45µW, passing the acceptance criteria.

Figure 5-2. Induced Voltage & Power from varying current within 100,200,300 turn coils with 24 AWG.

| 24 AWG Power Output | | | | | |
|---|---|---|---|---|---|
| Turns | Voltage (mV) | Power (µW) [1 mA] | Power (µW) [10 mA] | Power (µW) [100 mA] | Power (µW) [500 mA] |
| 100 | 1.611 | 1.611 | N/A | 161.1 | 805.5 |
| 200 | 3.045 | 3.045 | 30.45 | 304.5 | 1522.5 |
| 300 | 4.745 | 4.745 | N/A | 474.5 | 2372.5 |
| P/F | N/A | Fail | Pass | Pass | Pass |

Figure 5-3. Induced Voltage & Power from varying current within 100,200,300 turn coils with 30 AWG.

| 30 AWG Power Output | | | | |
|---|---|---|---|---|
| Turns | Voltage (mV) | Power (μW) [10 mA] | Power (μW) [100 mA] | Power (μW) [500 mA] |
| 100 | 1.614 | 1.614 | 161.4 | 807 |
| 200 | 3.165 | 3.165 | 316.5 | 1582.5 |
| 300 | 4.812 | 4.812 | 481.2 | 2406 |
| P/F | N/A | Fail | Pass | Pass |

Figure 5-4. Induced Voltage & Power from varying current within 100,200,300 turn coils with 30 AWG.

| 34 AWG Power Output | | | | |
|---|---|---|---|---|
| Turns | Voltage (mV) | Power (μW) [10 mA] | Power (μW) [100 mA] | Power (μW) [500 mA] |
| 100 | 1.526 | 1.526 | 152.6 | 763 |
| 200 | 3.227 | 3.227 | 322.7 | 1613.5 |
| 300 | 4.563 | 4.563 | 456.3 | 2281.5 |
| P/F | N/A | Fail | Pass | Pass |
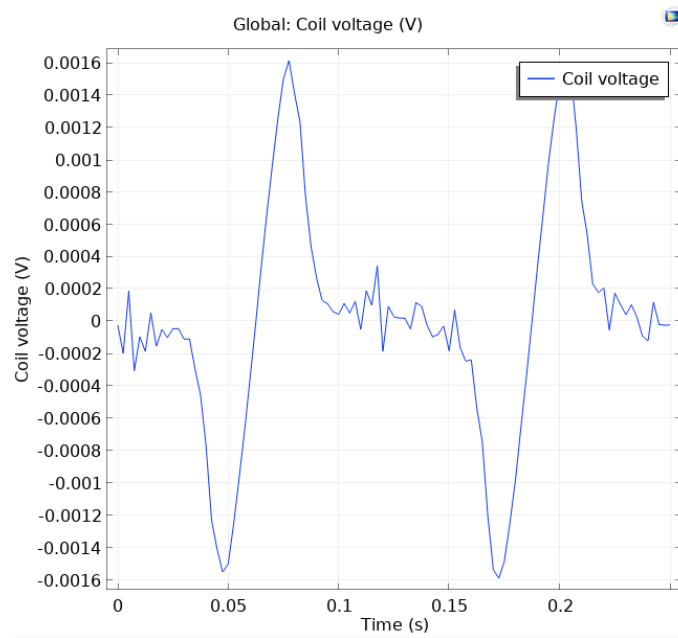
Figure 5-5. Induced Voltage Simulation Results

Conclusion:

As the number of turns increases, the voltage output increases as well. To meet the power acceptance criteria, a current higher than 10 mA needs to be generated. Further, a 10mm displacement provided a sufficient pathway to the most voltage. This study has some limitations for the understanding for the power output capabilities of the rechargeable pacemaker device. Because the device design includes two magnets, an inner one and an outer one, and this study only includes the inner magnet, it is not wholly sufficient to model the real-life device. However, it does provide information about base line voltage outputs which can be used to adjust the device.

## 5.3 Electromagnetic Thermal Analysis

<u>Purpose:</u>

FDA regulations pose a 2°C tolerance for the increase in blood temperature due to a medical device in the body. With inefficiencies built into any system, the resultant heat must be moderated COMSOL was utilized for its thermal analysis package to determine if the device would endanger patients with the use of this energy harvesting device.

<u>Acceptance Criteria:</u>

The acceptance criteria state that the blood surrounding the device cannot exceed 2°C more than human blood temperature, 37°C, a 312K limit.

<u>Abstract:</u>

A simple model of the pacemaker was made in COMSOL to simulate the temperature rise due to the moving magnet inducing a voltage in the coil after 10 hours. Moving blood was also placed around the model to simulate the moving blood in the heart that would surround the actual pacemaker. After different combinations of coil turns and casing materials, the pacemaker showed that it would not raise the blood temperature over 312K with 10mA in the device, a current specification set by the prior study.

<u>Background:</u>

According to Faraday's Law, when a magnet is run through a coil, a current is induced in the coil to oppose the change in magnetic field. When a current is induced in that coil, its temperature will rise due to the inefficiency of energy transfer. The materials

of the coil sheath were chosen for their known biocompatibility and ease of manufacturability these include: perylene C, Titanium, and 304 stainless steel.

Materials:

The program used to simulate this experiment was COMSOL 5.4 equipped with the thermal analysis kit.

Methods:

In COMSOL, a rectangle of width 3.35mm and height 25mm mimicked the Micra pacemaker and was defaulted to its specified outer material of titanium in a 2D axisymmetric model. Enveloping the Micra, a copper rectangle set to be the coils with variable turns and a .5mm offset (rectangle width of 4.85mm and height of 27mm) started the protectionary coil sheath made of variable material. another titanium rectangle of width 4.85mm and height 27mm. "Ampere's Law" and "Coils" physics were added to the simulation allowing 100, 200, and 300 turns were specified in the number of coils. 10mA was specified in the coil current as this was the optimal current found in the prior induced voltage study. The outer casing varied between titanium, 304 stainless steel, and perylene C. To simulate blood around the device, a temperature of 310K was set acting on the device at a frequency of 1Hz. Finally, a mesh was created, and studies were computed to observe the way the temperature around the coil was affected. The device was observed after 10 hours, sufficient time to see if a steady state equilibrium had been reached.

Results:

All combinations of coil turns, amps, and material passed the FDA regulation, never

rising above 311K displayed on figure 5-6.
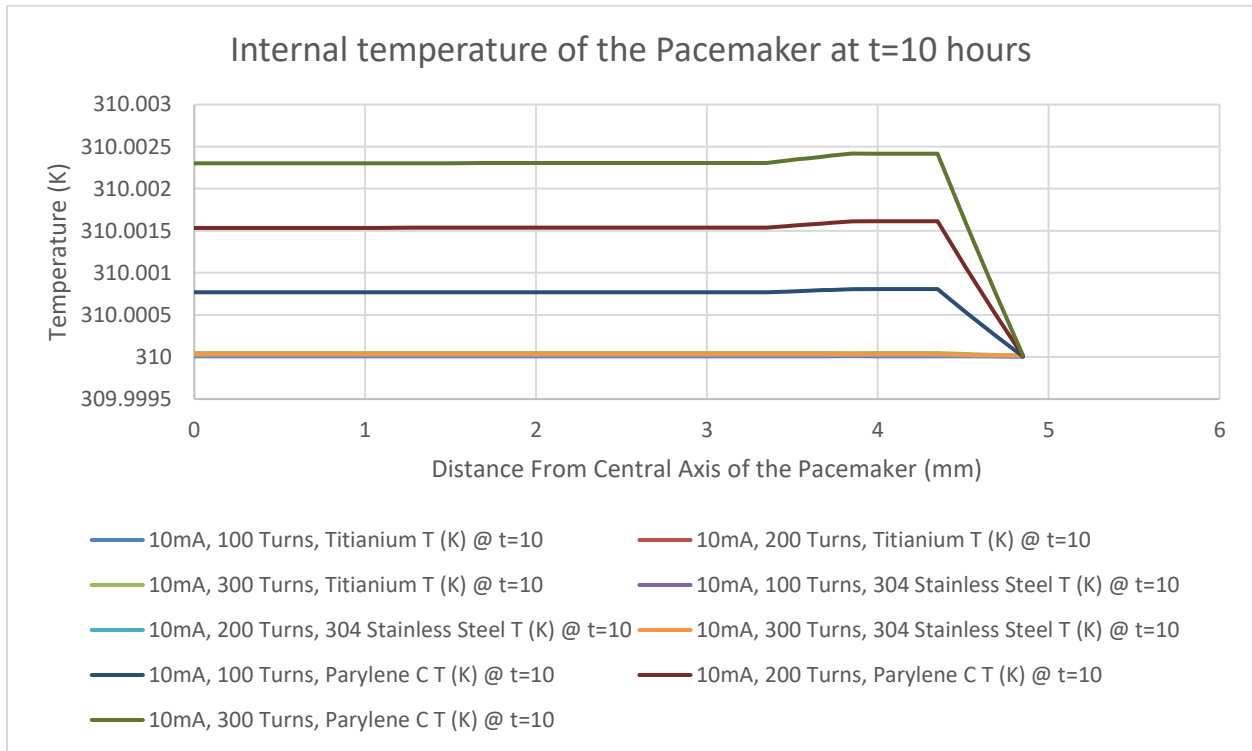


Figure 5-6. Electromagnetic Thermal Analysis Simulation Results.

With 10mA running through 100, 200, and 300 coil turns and titanium, 304 stainless steel, and perylene C casings the graph shows that the temperature of each case does not exceed FDA regulation. To note, the surface of the device would be found at approximately 4.75 mm however with the constant cooling affect, it would never exceed the 310 limits.

Conclusion:

All conditions passed the acceptance criteria of a <2°K increase. Further, all material choices originally listed, titanium, perylene C, and stainless steel would be considered acceptable for the design of the device.

5.4 Stent Displacement Analysis

Purpose:

The goal of this analysis is to simulate the displacement of the stents outer diameter along the central axis of the pacemaker. As noted earlier in the induced voltage simulation, the intend design of the stent consisted of a 10mm displacement of the stent with the permanent magnet located on its distal ring. By moving 10mm, as shown prior, COMSOL proved the capability of the system to produce 10 μW induced power enough to recharge the Micra pacemaker.

Acceptance Criteria:

The stent shall be displaced 10mm from its original starting position given a force equivalent to that produced by the ventricular wall.

Background:

To get to the final simulations described below, the team endured multiple versions that included utilizing Solidworks for its primitive simulations package. At first, utilizing the non-linear material of Nitinol caused significant lead times for simulation completion and inaccurate results. One possible reason for the failure may have been the production of

as one of singularities at the joints of the structures. To solve this, the model geometry was greatly simplified moving from a diamond pattern to a 2D axisymmetric version. For reference, the stent in its original shape is posted below and the 2D axi-symmetric version drafted for the simulation is shown.



A.



B.



C.
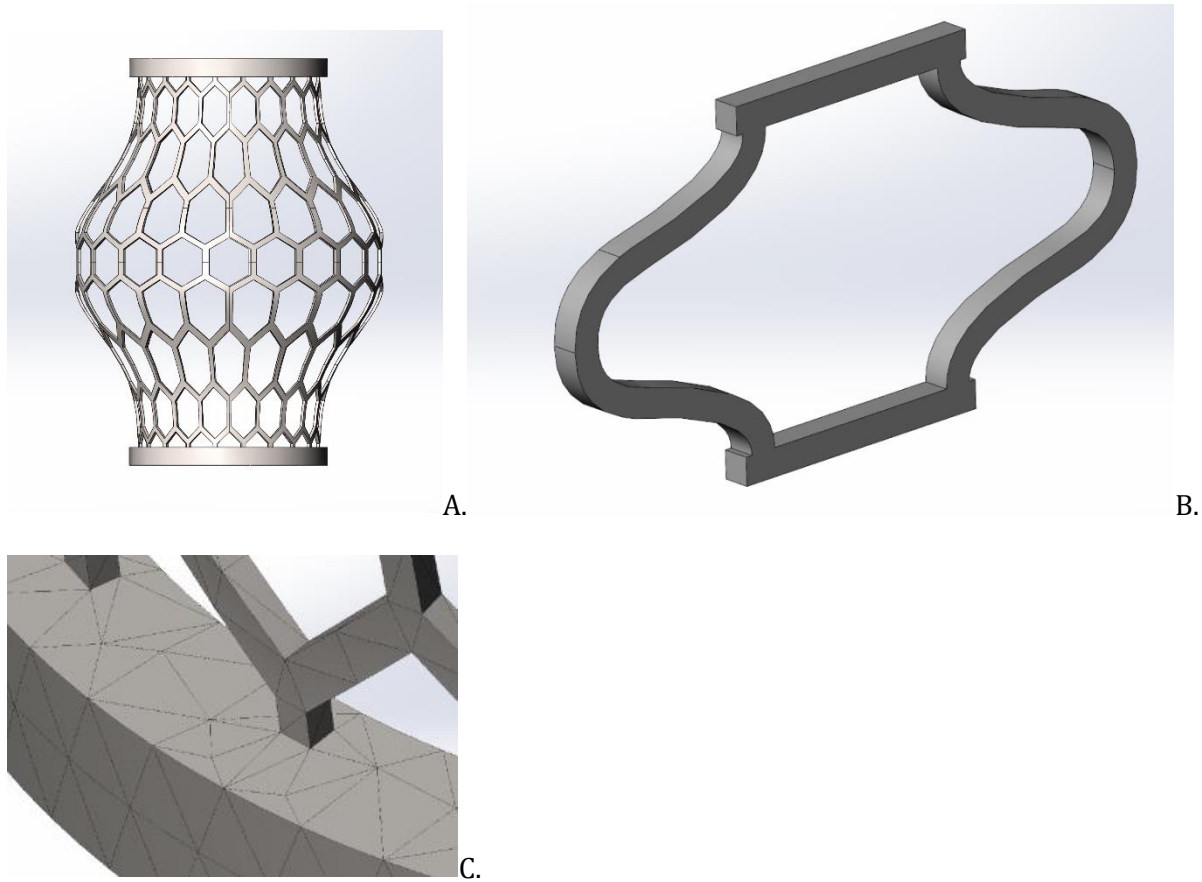
Figure 5-7. Mesh Compliance Simulation set up.

Where, the original stent design is shown in A, in B, the stent joints proved to be to computationally complex causing singularities to form in the simulation. Therefore a 2D -axis symmetric analysis was ran, which simplified the problem statement.

Table 5-6, the Nitinol material properties assigned in COMSOL.

| Property | Value | Units |
|---|---|---|
| Elastic Modulus | 83000 | N/m^2 |
| Poisson's Ratio | 0.33 | N/A |
| Shear Modulus | 10800 | N/m^2 |
| Mass Density | 6450 | kg/m^3 |
| Tensile Strength | 895 | N/m^2 |
| Yield Strength | 100 | N/m^2 |
| Thermal Conductivity | 10 | W/(m*K) |
| Specific Heat | 0.32 | J/(kg*K) |

Methods:

Within COMSOL a 5000N load on the side of the stent. A 2D-axi symmetric model was created with a split line located 3mm from the top and bottom of the stent. This split line would act as the area which the force could be applied upon. Fixtures for the simulation only included a fixed bottom surface at the proximal end of the stent. The total height of the stent was 12 mm with an initial width of 5mm (chosen to fit within the normal apex of a human heart) and a thickness of 1mm. This may be summarized in the tables X/Y below. Aluminum was set as the material for the ends (where the distal magnet holders would be) while the rest of the body shown in blue in figure 5-8 was set as nitinol.
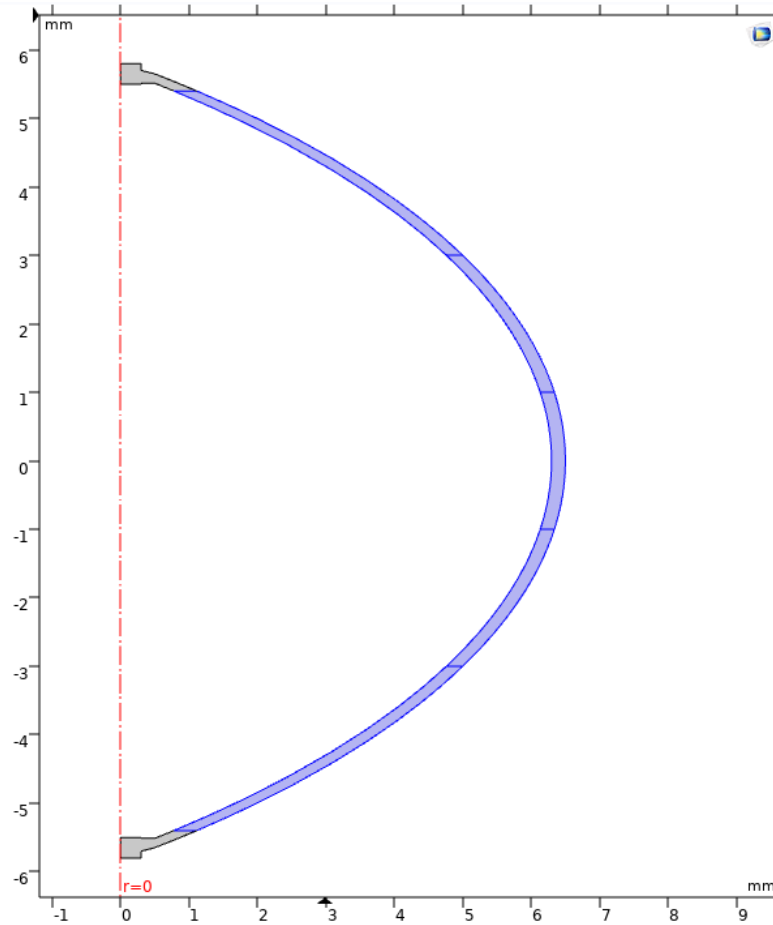
Figure 5-8. The Mesh Simulation geometric set up in COMSOL.

Figure 5-9. The Mesh Simulation key input data in COMSOL.

| Material | Fixtures | Force | Partition Area |
|---|---|---|---|
| Nitinol (Blue) ,Aluminum (Gray) | Fixed bottom left contacting surface | 5000N in the X direction | Middle (Top +3mm, Bottom -3mm) |

## Results:

After multiple iterations, it was only in the 5000N condition which was a 16x gain from the 300N prescribed in the above that a 10mm displacement was achieved. However, this failure may due to the following (1) the 2D axis Symmetry simplification or (2) the parameters of the stent. 2D axis Symmetry, when rotated into its 3D shape that the analysis would account for fails to include the porosity of the diamond cuts that were initially intended to decrease the stiffness and increase the elongation of the stent. To visualize the simplification problem a prior iteration derived from Solidworks is shown in Figure XX displaying the lack of porosity. Secondly, the parameters of the stent, i.e its thickness, height and width may also need to be adjusted in the further studies to better compensate for a 10mm displacement.
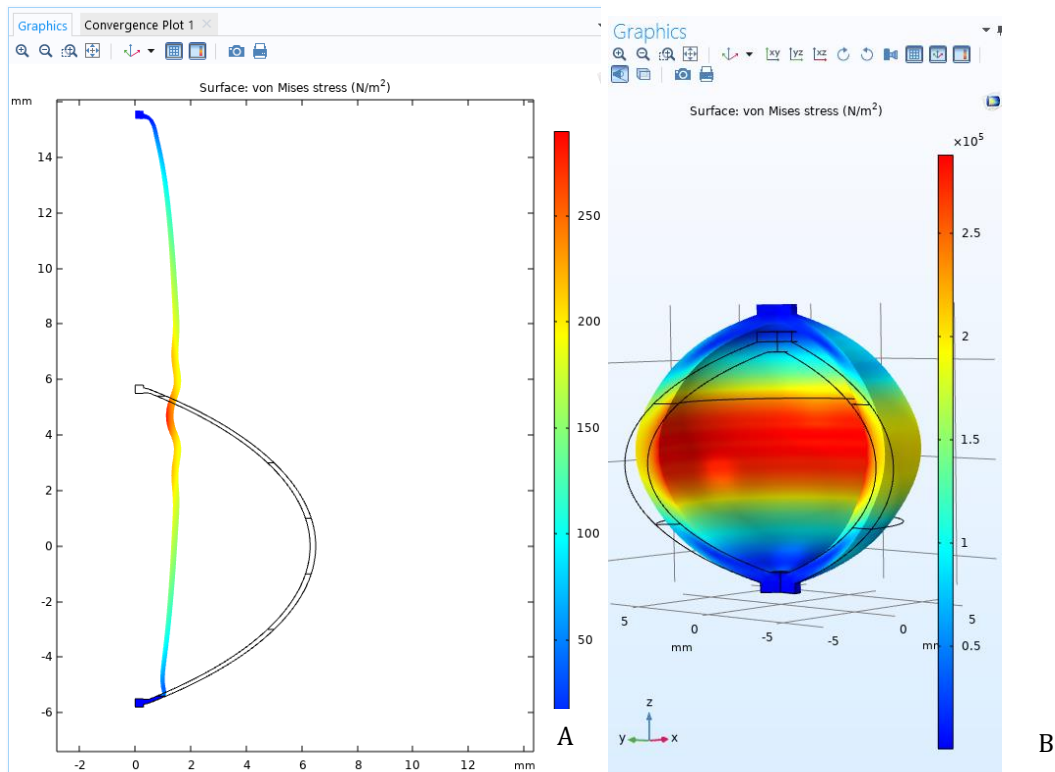
Figure 5-10.The Mesh Simulation geometric results COMSOL.

In A, a 5000N load was applied so that a 10mm displacement would occur. Given the minimal expected force (30N) the displacement was significantly less as seen on the right by the axis resolution.

## 5.5 Modal Analysis

Purpose:

Using Solidworks, a modal analysis shall be conducted to analyze the fundamental frequency of using the uniquely formed "stent". Importantly, if a fundamental frequency is found at the 1-2 Hz range, the device shall likely to cause it to vibrate to a point where it would break during prolonged use.

Acceptance Criteria:

1-2Hz shall not be found as a fundamental frequency.

Abstract:

A modal analysis was conducted via Solidworks frequency analysis software within its Simulation package. Upon inspection of the outer stent, the first five modes found to be fundamental frequencies were well above the operating Hz of the device thus, the device is deemed safe, from a vibrational perspective, for application.

Background:

The importance of finding the fundamental frequency is derived from the mathematical analysis of a spring/damper system. In it, as seen below, if a mass is forced or

moved, it will cause an excitation along the spring and a recoil is imminent. However, by

applying the correct frequency to the system a large amplitude of oscillation will be

produced that may prove to be catastrophic to the system.

Where:

$k$: Spring stiffness
$m$: Mass
$c$: Damping coefficient
$F(t)$: Input force
$F_0$: Maximum amplitude of the input force
$\omega$: Input frequency
$x(t)$: Displacement of the mass
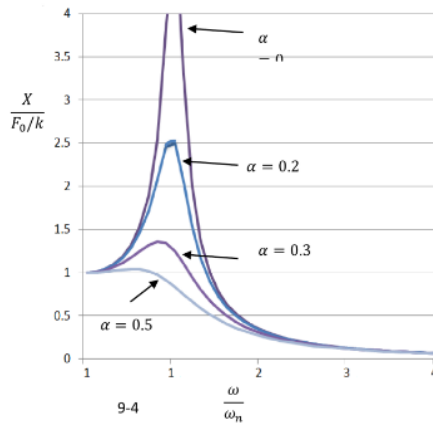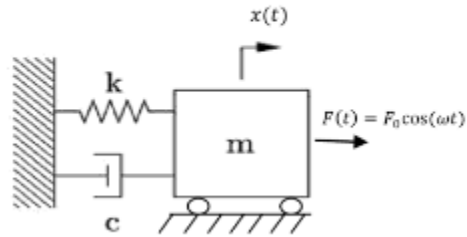


Figure 5-11. Modal Analysis Fundamentals.

In A, the mass and damper set up that provides the basis for deriving the fundamental frequency. B, the heightened movement is displayed when a system reaches its harmonic or fundamental frequency in comparison to other systems especially in under damped systems.

Sources: Adapted from [52]

76

Materials:

Solidworks 2018-2019 for the computation software for this simulation along with the academic license to allow access to the simulation package.

Methods:

Nitinol was applied as the material for the stent with a fixture located at the bottom face of the lower ring to mimic how the stent would be attached to the Micra. No external forces were applied as to not alter the vibration study. To visualize the test set up, a screen shot of the Solidworks stent model along with its first deformation is found below.
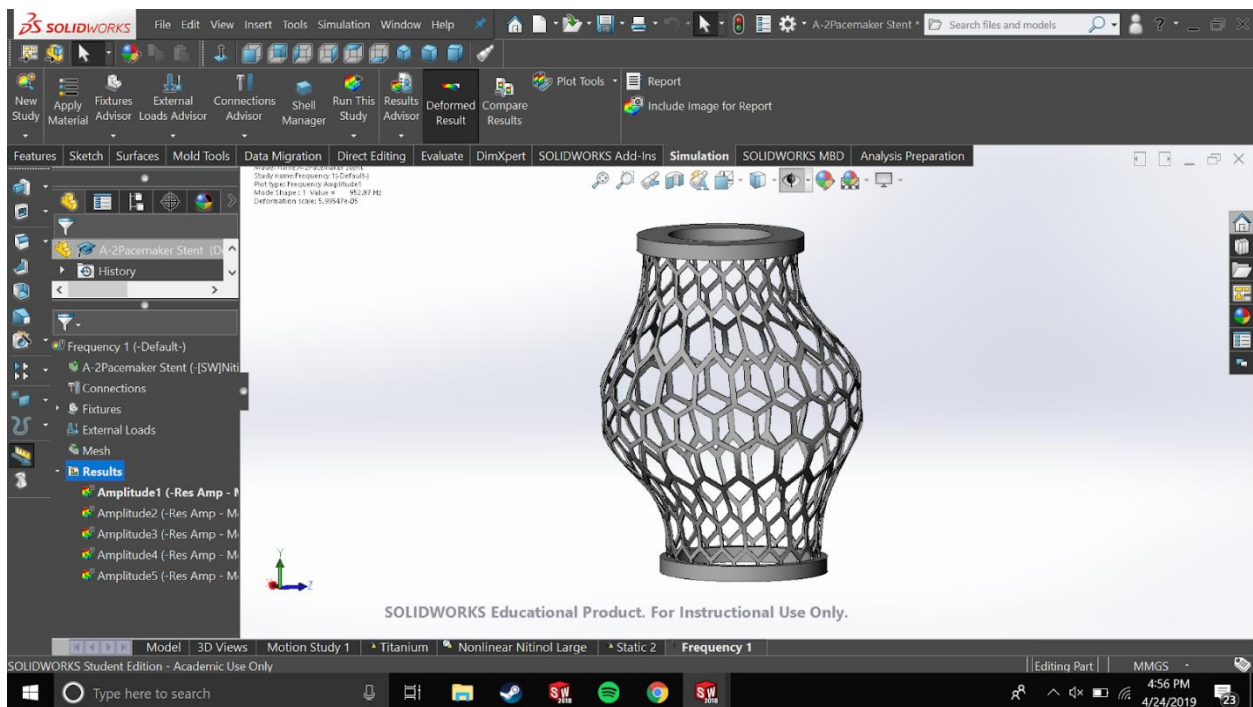


Figure 5-12.Modal Analysis Stent Design Set up.

Results:

No fundamental frequencies were found in the 1-2 Hz range, with the nearest resonant frequency being at 952 Hz. Thus, well above the operating conditions of the

77

device. To support the repeatability of the simulation study, the model's details are have been copied below.

Figure 5-8. The Modal Analysis Output- Fundamental Frequencies of the system.

| Mode No. | Frequency (Hertz) |
|----------|-------------------|
| 1 | 952.87 |
| 2 | 955.44 |
| 3 | 2323 |
| 4 | 6262.5 |
| 5 | 6279.2 |

Figure 5-9. Modal Analysis Mesh Parameters

| Study name | Frequency 1 (-Default-) |
|------------|-------------------------|
| Mesh type | Solid Mesh |
| Mesher Used | Standard mesh |
| Automatic Transition | Off |
| Include Mesh Auto Loops | Off |
| Jacobian points | 4 points |
| Element size | 0.300763 mm |
| Tolerance | 0.0150381 mm |
| Mesh quality | High |
| Total nodes | 93569 |
| Total elements | 45528 |
| Maximum Aspect Ratio | 37.3 |

Conclusion:

No fundamental frequency were found in the 1-2 Hz range and thus it meets the original acceptance criteria.

# Chapter 6 - Magnetic Core: Benchtop Tests

6.1 Induced Voltage: Linear Actuator

<u>Purpose:</u>

With the simulated results generated from COMSOL of a 2-5mV generation on the 1:1 scale the next item to test was the hypothesis of the utility of a double magnet (outer magnet around the electrical coils with an inner magnet) for electromagnetic generation on the large 3:1 scale. The goal of the study was twofold, (1) to test the double magnet mechanism where an outer magnet would be actuated and the inner magnet would be dragged by the outer magnets pull and (2) to test the output voltage given a 3:1 scale

<u>Acceptance Criteria:</u>

The acceptance criteria for this experiment is a generation of at least 10 µW of power or 5mV.

<u>Materials:</u>

This setup utilizes customized 3D printed parts, our coil device, threaded rod with nut, motors, and an Arduino relay. A threaded rod and nut was used and attached to a coupler. The coupler was then attached to a 24V 3000rpm DC motor. Customized 3D parts were made based on the dimensions of the materials used. An Arduino relay was hooked up to the linear actuator, programmed by Arduino code. The materials used for this experiment were copper wires, two magnets of different diameters, masking tape, and a 3D

printed hollow cylinder. The large magnet has an outer diameter of 2 inches with and inner diameter of 1 inch. The small magnet has an outer diameter of ¾ inch and an inner diameter of 7/16 inch. The hollow cylinder consists of an inner diameter of 13/16 inch and an outer diameter of 15/16 inch. This cylinder was 3D printed with the specific dimensions in order to fit both the large and small magnets. The copper coil was made from a polyurethane enameled copper wire of 34 AWG.

Methods:

The linear actuator was designed using rotation movement that would translate to translational movement. The nut that was fastened to the threaded rod was secured onto a customized 3D printed part which would stabilize the nut giving it a translational movement. Other customized 3D parts were used to secure the coil device to the linear actuator and was used to guide the movement of the outer magnet. The coils were held stationary on the other side and only the outer magnet interacted with the linear actuator. The Arduino relay allowed for oscillating movements, switching the direction of the linear actuator moving forwards and backwards to complete an approximate 30mm path at 1-2Hz. The linear actuator device controlled the movement of the outer ring magnet and oscillated the magnet over the coils at a constant frequency. A Solidworks rendering is provided below to show the set up of the linear actuator and the final prototype used. 10 trails were completed and recorded utilizing an oscilloscope for (1) the control condition of no movement, to check for current or voltage noise and (2) the variable condition where the linear actuator would be activated.

A

B
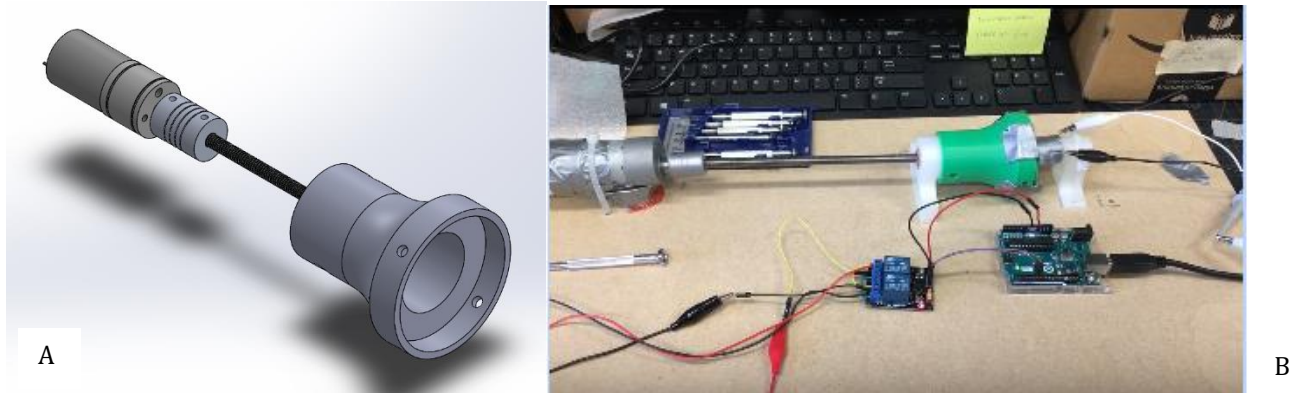
Figure 6-1. Induced Voltage Benchtop Set up.

Including the CAD renderings of the custom linear actuator (A)and the actual set up (B). A Custom set up was used to manipulate the outer magnet.

Results:

Below, the graph shows both the voltage and current during variable and control conditions. Notably, the test-set exhibited a large noise over both the current and the voltage outputs likely attributed to the small gauge wire (34AWG) that was difficult for the oscilloscope alligator clips to attach to. Regardless, a significant increase in the variable condition was found where an average voltage of 232 mV was obtained and a current of 100 mV

## Linear Actuator Results
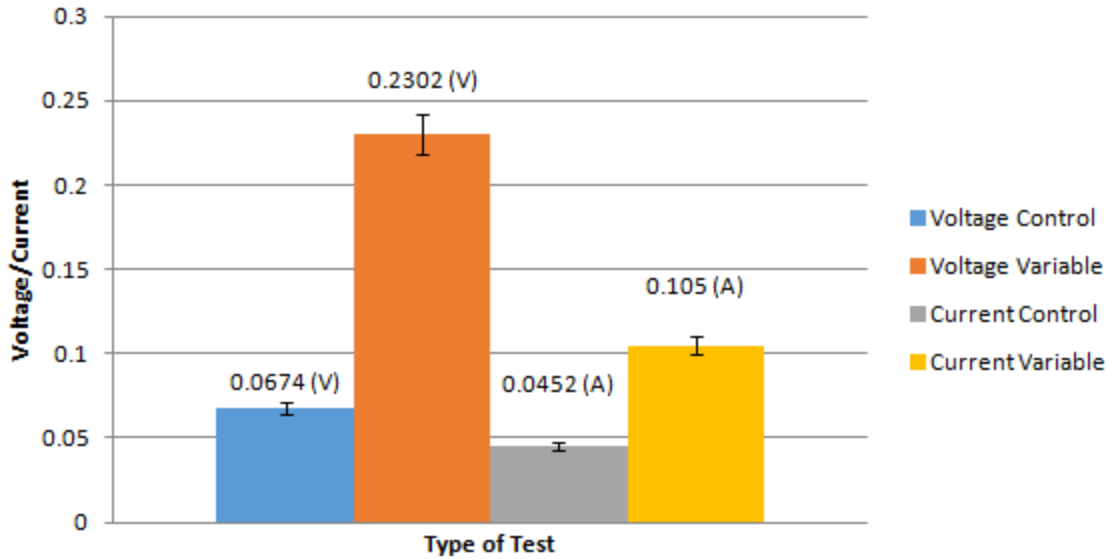


Figure 6-2.Induced Voltage Benchtop Ouputs.

Both current and voltage are shown, where the average voltage over the 10 trials was 230 mV far surpassing the acceptance criteria even given a 3x scaling.

Conclusion:

As proven from the manually actuated experiment, electromagnetic induction of two concentric magnets is functional. The linear actuator test confirmed that with a double magnet system it would be possible to harvest more than ample energy for the device. With an output of 0.2302 V, this greatly exceeds the acceptance criteria of 10 μW or 5mV calculation even with the 3x gain factor applied to the system.

6.2 Magnetic Shielding

Purpose:

The purpose of this test was to see if copper foil was able to shield a mock pacemaker from the magnetic fields produced by surrounding magnets. This experiment is

important to the team's progress on the device, as normal pacemaker function is severely affected by near external magnetic fields.

Acceptance Criteria:

The main goal of this proof experiment was to attempt to reduce the initial magnetic field read by the gaussmeter with no magnetic shielding by initially 75% and then 90% during the second test method. Given the relatively low magnetic permeability of copper ($1.26*1-_6$ H/m), we hypothesize that the copper shielding will aid a small amount in shielding the magnetic field from the gaussmeter.

Abstract:

The ring-magnet design created to induce electromagnetism generated a magnetic field capable of interfering with the pacemaker device nested inside the magnets. To overcome this obstacle, magnetic shielding in the form of different metals coatings were investigated. Nickel foil of width 0.12mm and a MuMetal sheet of width 0.06mm were wrapped around a mock pacemaker and the magnetic field inside was measured with the inner and outer ring magnet setup. Nickel and MuMetal were chosen because of their relatively high magnetic permeabilities. Results showed a positive effect on magnetic shielding with the Nickel and MuMetal shielding

Background:

Magnetic shielding is a method used to redirect magnetic fields from an area of unwanted fields. The most popular materials used in magnetic shielding are called

ferromagnetic materials. Alloys containing Iron, Nickel, and Cobalt also work great as shields. The magnetic permeabilities of copper, nickel, and MuMetal are $1.26*10_{-6}$, $1.26*10_{-4}$, and $2.5*10_{-2}$ respectively. The underlying hypothesis was that the effectiveness of shielding would correlate with the increase in magnetic permeability; with MuMetal being the most effective shield and Copper being the least effective shield. Thickness of shielding is also a factor in the amount of the magnetic field that makes it through the shield. The link below links to a nice gif that gives a visual representation of the amount of deflected field as the thickness of the shield varies.



A        B
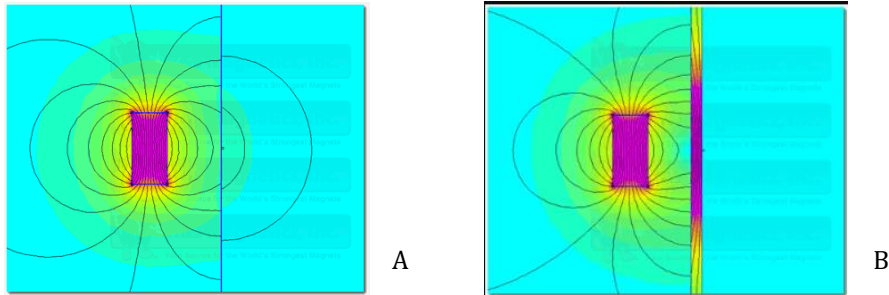
Figure 6-3. Magnetic Shielding.

Provided by K&J Magnetics, as the thickness of the magnetic shielding increases the ability to disrupt or shield increases. The key material property magnetic permeability thus plays the largest role in determining what thickness would be sufficient to block a substantial amount of the magnetic waves.

Source: Adapted from [53]

Materials:

Materials used in this test included adhesive copper foil, an F.W. Bell 5100 series Hall Effect Gauss/Tesla Meter, a ½'' x ¼'' x ⅛'' N52 grade neodymium ring magnet, a 3/2'' x 3/4'' x 1/8'' N52 grade neodymium ring magnet, a hollow mock pacemaker and a 3D printed cylinder, with an inner diameter of 13/16" and an outer diameter of 15/16". spacer between the concentric ring magnets.

Methods:

The experimental setup was as follows: a gaussmeter was used to measure the

magnetism in the setup, copper foil was wrapped around the pacemaker and the device

was placed inside of 2 concentric ring magnets. The gauss values were recorded 8 times

per material. A control test with no magnetic shielding was also performed. Between trials,

the gauss meter was calibrated and zeroed. Lab stands and tri-grips were used to stabilize

the gaussmeter and the magnet setup. This was to avoid wildly fluctuating values that were

read by holding the probe by hand pre-testing. The distance the probe was inserted into

the mock device was kept constant through measuring the distance before each test.



Figure 6-4. Benchtop Set up for the Magnetic Shielding Experiment.

 Where a 3D printed coils and an inset key slot for the gauss meter maintained the reliability of the experiment as the 3D print constrained the meter.

Results:

The results of the mag-shield testing with copper are show in the boxplot above. It is

clear that the copper foil played a large role in deflecting the magnitude of the magnetic

field picked up by the gaussmeter. By examining the median values taken with the shielding and with the control, the shielding passed the original acceptance criteria with approximately 83% reduction of the mag-field. Then during the second version of the test where Nickel and Mu-Metal were tested, the results showed a 93% reduction of a magnetic field again passing the test criteria.
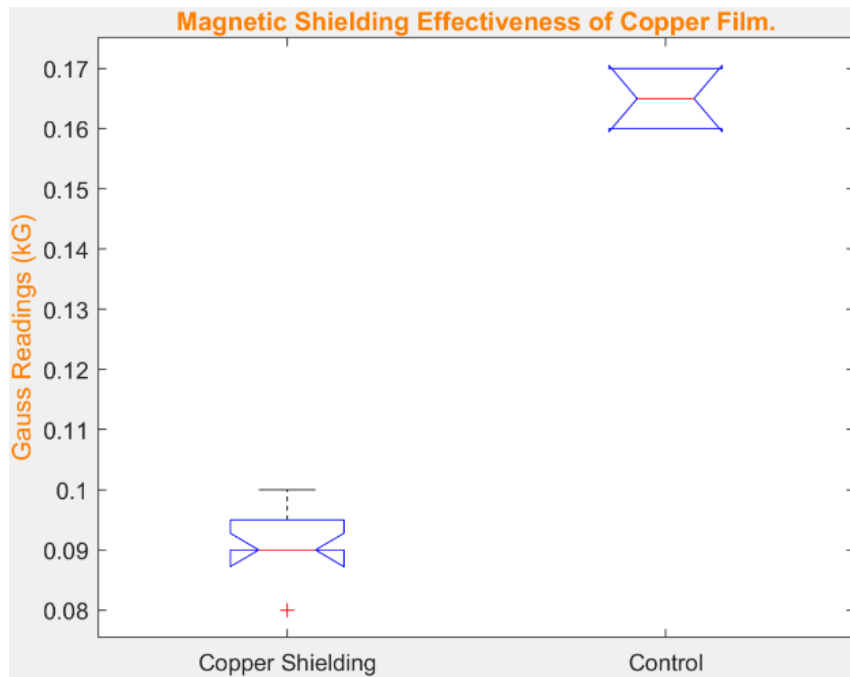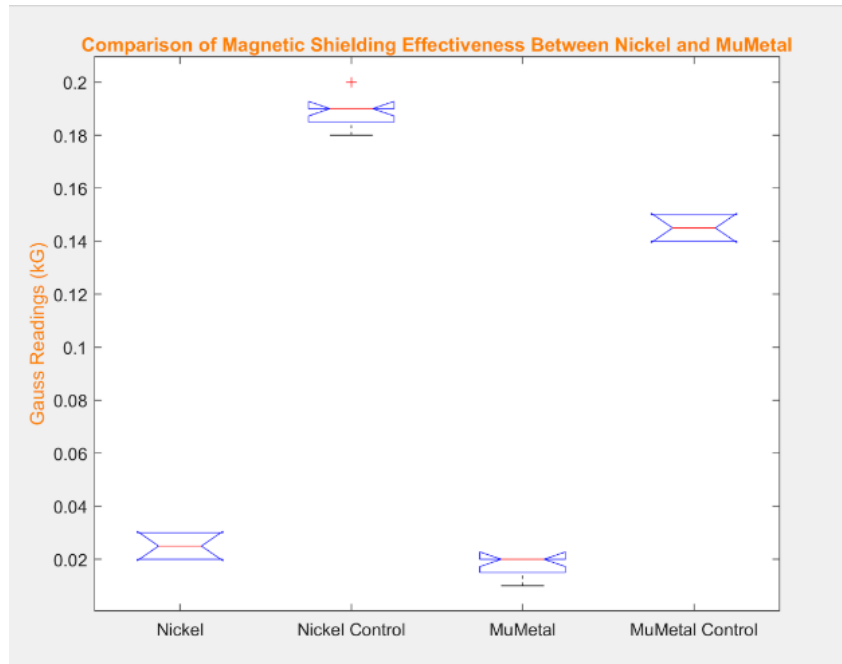
Figure 6-5. Magnetic Shielding Results.

Where the additional material significantly decreased the magnetic field expressed in the center of the coils i.e where the Micra pacemaker would sit. Here the results are split, Copper/ MuMetal/Nickel as the copper test was ran first with a preliminary acceptance criteria of 75% reduction in magnetic field and then later the test was retried with stricter standards of a 90% reduction

Conclusion:

From the results, the team concludes that Nickel and MuMetal are effective as magnetic shielding elements with regards to the proposed device. The initial acceptance criteria was met and exceeded by each shielding element in its respective test. The Nickel has an average Mag Field reduction of 84%, and results from MuMetal readings gave between 85-93% Mag Field reduction. This trend between the two materials follows the original supposition that MuMetal would perform better than Nickel due to its higher magnetic permeability.

6.3 Magnetic Pull Force

Purpose:

   The purpose of examining this problem was to see whether the concentric ring magnet setup would remain together when subjected to the inertial force from rapidly traverse from the distal orientation to proximal during the pulsatile oscillations within the heart.

Acceptance Criteria:

   The force holding the two ring magnets to each other must be at least 2 orders of magnitude greater than the inertial force that the magnets are subjected to by the impulse caused by sudden change in direction.

Abstract:

   Proof of concept research and hand calculations will be conducted in order to ensure that the magnetic force is greater than the inertial force of the inner magnet.

Background:

   Two concentric ring magnets (with a tightly wound copper coil in between them) are oscillated up and down a linear track. The goal of this motion is to induce an electromagnetic field. The proposed device will be placed within a heart chamber that has a beat frequency of 1 Hz. The inner magnet must be able to stay within the larger outer magnet at the top and bottom of the periodic oscillations. In order for the inner magnet to

stay in place, the force due to its inertia must not overcome the force between the magnets themselves.

Methods:

The primary equation than describes the impulse of a moving object is as follows:

$$F = m\frac{\Delta v}{t} \hspace{4cm} (6.1)$$

Where $F$ is the force, $m$ is the mass of the object, $\Delta v$ is the change in velocity, and $t$ is the time of impulse. In this particular application, two 3x scale ring magnets were used. Both were N52 grade neodymium ring magnets. The larger outer magnet had specifications: 1" OD x 1/2 " ID x 1/8" thick. The smaller inner magnet had specifications 1/2" OD x 1/4" ID x 1/8 " thick. The pull force rating for the big and small magnets were 11.2 and 6.6 pounds of force respectively.

Doing the calculation, $m$ is the mass of the magnet setup, which is 2.26 g. $T$ is the time it takes for each oscillation is approximately 0.5 seconds. $V$ is equal to the distance the magnets travel divided by the time it takes for them to travel; the distance travelled is taken from the scale model, which is 28 mm, and the time is equal to half a second.

Results:

Applying the impulse equation and the information we have; we get that the inertial force due to impulse on the system is equal to approximately $5.69 * 10^{-5}$ pounds of force.

Conclusion:

This force is more than 2 orders of magnitude less than the force of the larger magnet, which was 11.2 pounds of force. Thus the experiment passes the original acceptance criteria.

6.4 Animal Study

Purpose:

      To test if the proposed device could reasonably fit inside the ventricle of a heart, a pig's heart was obtained, and different 3D models were inserted. The dimensions of the device must be designed to fit inside the heart because otherwise, a large device could disrupt heart function potentially harm patients.

Acceptance Criteria:

      The device should reasonably fit inside the heart without stretching or ripping the muscle fibers.

Abstract:

      4 models were tested inside the heart: solid shell, four strip shell, chubby, and two times scale model. The solid shell, four strip shell, and chubby models all passed the acceptance criteria: they easily fit into both the left and the right ventricles of the heart. The two times scale model did not pass the acceptance criteria as it was too large.

Background:

      The heart is made of four chambers, the atriums (right/left) and the ventricles (right/left). Atriums act to receive blood from either the body (right) or from the lungs (left) while the ventricles send this blood out to the body(left) or the lungs(right) to be

oxygenated. Here the left ventricle is measured for its size and volumetric capabilities to store an energy harvesting device.
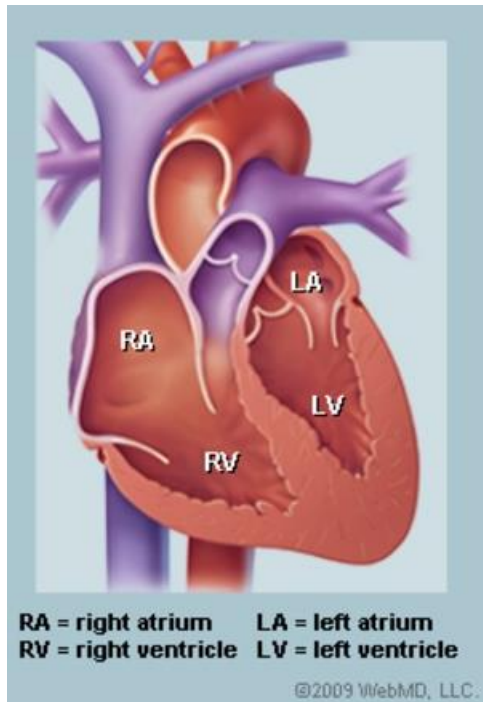


Figure 6-6. A diagram of the four chambers of the heart.

Source: Adapted from [54]

Materials:

The models were design on Solidworks 2018 and 3D printed with an IIIP 3D printer with PLA filament. While the pig heart was supplied from a local H-mart.

Methods:

The top half of the pig's heart was cut and removed. Each model was then inserted into the open left and right ventricles to test the dimensions. Then the same pig's heart was inserted in the heart pumping fixture a twisting motion was performed by hand to visualize

how the device would work. Afterwards the pig heart was examined for the inner dimensions for future reference.

Results:

When inserted into the left ventricle of the pig's heart, the solid shell, four strip shell, and the chubby models all fit with ease. The model and the muscles walls made contact but the device easily slid into the chamber. The two times scale model could technically be inserted into the left ventricle, however, great force was needed and the muscle fibers were stretched and started ripping. In addition, the two times model could not be inserted fully length-wise. This confirmed the feasibility of our prior set dimensions.

Table 6-1. Animal Study Result Pictures.

| Model | Pictures |
|-------|----------|
| Solid shell |  |

| | |
|---|---|
| Four strip shell |  |
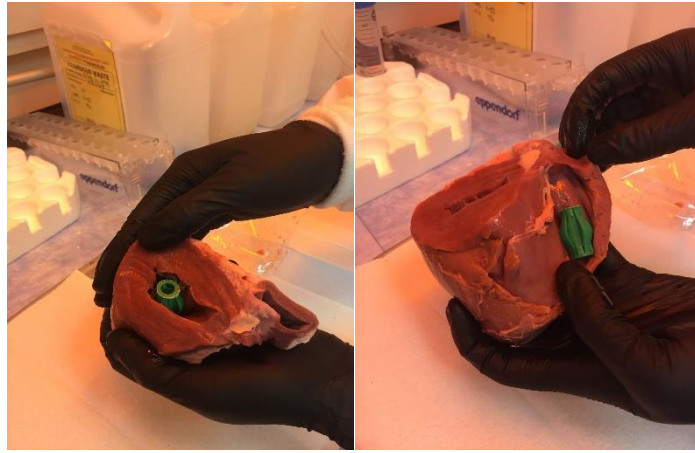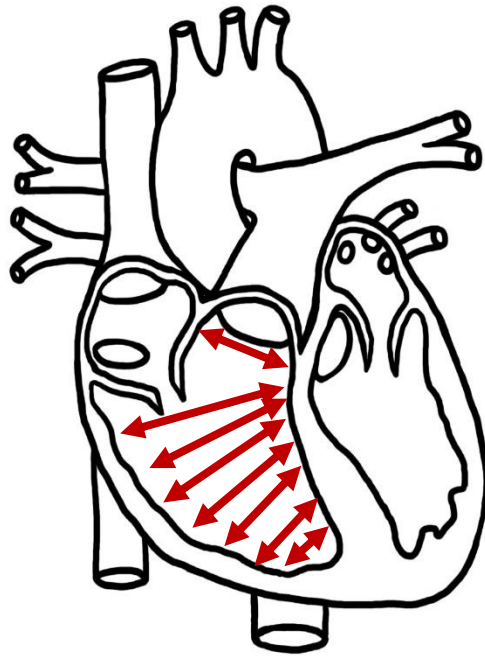
Figure 6-7. Left Ventricular Measurements -Swine Study.

Source: Adapted from: [55]

Figure 6-8. Dimensions of a Pig's Heart (Left Ventricle) diagram of the four chambers of the heart.

| Dimension (Descending) | Value [cm] | Description |
|---|---|---|
| 1 | 2 | Pulmonary Valve Diameter |
| 2 | 9 | Pulmonary Valve to outer wall |
| 3 | 4.5 | Left Ventricle |
| 4 | 3.5 | Left Ventricle |
| 5 | 4 | Left Ventricle |
| 6 | 3 | Left Ventricle |
| 7 | 2 | Left Ventricle |
| 8 | 0.7 | Apex |

Conclusion:

The one scale models passed the acceptance criteria and the team obtained valuable data of dimensional accuracy. Although it must be noted that a big heart is notably larger than a human heart, as a rough prototype, it showed that the device size was plausible.

6.5 Electromagnetic Thermal Analysis

<u>Purpose:</u>

Because the FDA regulates that a medical device cannot raise the temperature of the surrounding tissue more than 2℃, this test serves to demonstrate whether the heat and temperature increase from the friction of the magnets rubbing on the device will meet that criteria.

<u>Acceptance Criteria:</u>

The temperature probe inside the device with sprayed water over it should not exceed 39℃, 2℃ above body temperature.

<u>Abstract:</u>

The FDA requires all implantable devices to stay within 2℃ (+/-) of body temperature, 39℃, to ensure the safety of the patient. In order to investigate the issue of thermal increases due to friction forces in the oscillating magnet system, a simple experiment was designed, and data was compared to the 39℃ upper thermal limit dictated by the FDA. Results found that while a control test saw a ~5-7℃ temperature change, the same test run with water temperature water as a coolant saw smaller changes in comparison. In all three water test trials, the temperatures did not exceed 2℃ from the initial measurement.

During experimentation, it was noted that the magnets were unable to maintain an optimum concentricity and thus the inner magnet continually moved toward one side. This of course was a point of concern particularly for heat generation caused by the friction of the two surfaces. This is phenomena detailed below underlines the issue.
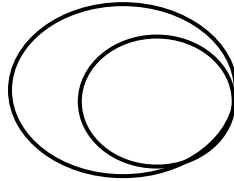
Figure 6-9. Electromagnetic Thermal Testing – Root Cause.

A basic figure that shows the underlying problem with the double magnet system where one magnet would continue to rub against the other, sparking the initial concern and need for the study.

## Materials:

For the heat generation testing, three main materials were used: PDMS, two concentric magnets, and a thermocouple. In order to set up the experiment, a 3D-printed hollow cylinder was used that was made to fit the outer diameter of the inner magnet, with an inner diameter of 13/16" and an outer diameter of 15/16". Two 3x scale ring magnets were used. Both were N52 grade neodymium ring magnets. The larger outer magnet had specifications: 1" OD x 1/2" ID x 1/8" thick. The smaller inner magnet had specifications 1/2"OD x 1/4" ID x 1/8" thick. A thin layer of PDMS of 0.75" surrounded the 3D printed cylinder. An outer magnet was positioned to fit around the PDMS layer and the cylinder. The thermocouple was placed on one end in between the PDMS layer and the cylinder and was secured using electrical tape.

For the water testing, a similar list of materials was used in addition to a 6 L/min peristaltic pump and a hot plate to pump the water and maintain the temperature at around body temperature.

Methods:

The control setup of the experiment was primarily just testing the heat generated from the magnets against the PDMS. The outer and inner magnets were oscillated manually across the height of the hollow cylinder for 15 minutes. The thermocouple acquired the temperature change throughout the time frame. Three trails were conducted per the control (without water) and variable (with water).

Similar to the control setup, the trials with water were conducted by manually oscillating the inner and outer magnets over the PDMS covered cylinders for 15 minutes. A thermocouple was placed under the PDMS surface of the cylinder and in the water tank and the temperature was recorded throughout the trial. A 1000 mL beaker filled with water was maintained at a temperature of 38℃ using a hot plate. Warm water was pumped from the beaker at 100 mL/min and sprayed over the manually oscillating magnet-cylinder setup. More warm water was periodically added to the beaker as the trial went on to keep the temperature constant.

Results:

From the control experiment, the change of temperature ranged from 5-7℃. The first run started at 23.4℃ and increased to 29.1℃ after 15 minutes, resulting in a 5.6℃ temperature change. The chart below shows the change in temperature for each of the four runs with its starting temperature and ending temperature after 15 minutes. Calculating

the average change in temperature during the control (with no water) would be 6.06°C.

While with water the temperature dropped to acceptable levels of 1.1°C change in

temperature. Of course, the question must raise if 15 minutes would be a long enough time

to determine if the system had reached equilibrium. However, by viewing the output

graphs from the thermocouple, after initially heating from room temperature, the surface

temperature quickly reaches equilibrium and only slightly if at all alters.

Figure 6-10. Temperature Testing Control Variable Results (No Water)

| Run | Starting Temperature °C | Ending Temperature °C | Change in Temperature °C |
|---|---|---|---|
| 1 | 23.4 | 29.1 | 5.6 |
| 2 | 23.6 | 30.4 | 6.8 |
| 3 | 24 | 29.8 | 5.8 |

Figure 6-11.Temperature Testing Variable Results (6L/min Water)

| Run | Starting Temperature °C | Ending Temperature °C | Change in Temperature °C |
|---|---|---|---|
| 1 | 29.9 | 31.4 | 1.5 |
| 2 | 33.4 | 35.1 | 1.7 |
| 3 | 34.6 | 34.7 | 0.1 |

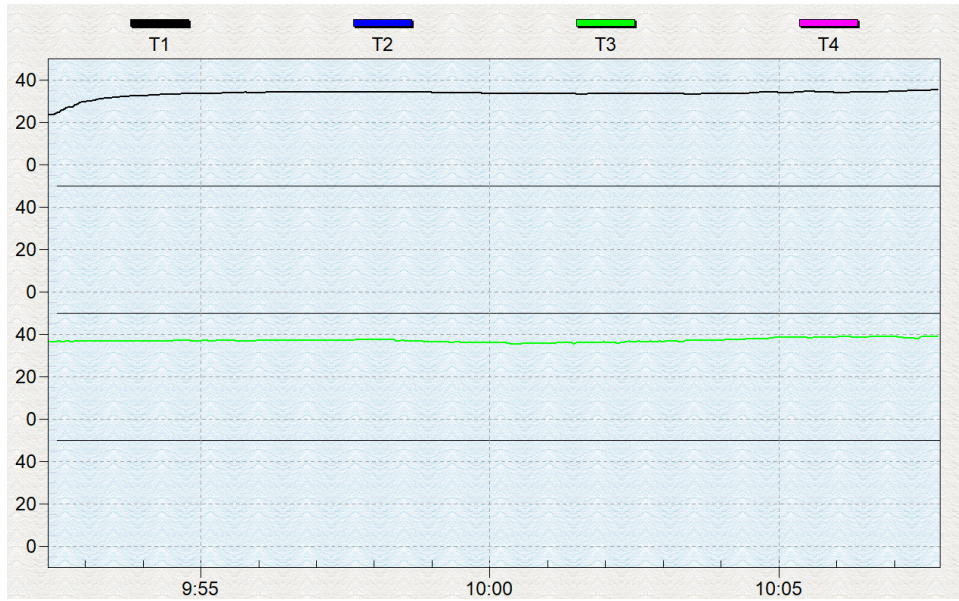Figure 6-12.Temperature Testing Control Variable Results (No Water)

Figure 6-13.Temperature Testing Benchtop Results.

Displayed here are the data from one of the tests with the 6L/min pump. Water was stored at a constant body temperature shown in green (or T3) and the surface temperature (T1), little to no temperature fluctuations are seen during the trials.

# Chapter 7 - Summary and Conclusions

7.1 Intellectual Protection

 The ideas captured in this thesis shall be incorporated in a provisional patent and with the proper funding and advancements the ideas are intended to be solidified in a utility patent.

7.2 Concluding Remarks & Future Works

 Two years of research mark an end to a lengthy study on novel energy harvesting techniques where a novel blood flow sensor for stents was examined along with a rechargeable pacemaker design. In the end, both designs have proven feasibility. Of focus, the rechargeable pacemaker design has three significant future considerations: (1) stent deformations, (2) fatigue studies , (3) and blood clotting. In the stent deformation results, the 5000N requirement for a 10mm offset proved that either a redesign or a simulation modification was needed. One of the possible ideas the team referenced is to return to a serpentine cut for the outer stent, shown again for reference. The design has the potentiality to have higher elongation as the serpentine struts would be parallel with the direction of intended expansion. Potentially, such a design could lead to higher fatigue rates and thus, is noted for future works. Secondly, the magnet/magnet interactions mentioned in 6.7 were of concern for team as, the constant rubbing on the surface between the PDMS sheath and the magnet are likely to cause failures on either the magnet or the surface of the sheath. To test this, the team has begun experimenting with Solidworks once more to establish a simulation to test the lifetime of the PDMS under such a force. The initial setup may be seen in the figure 7.1, where a fixture is placed upon the upper lip of the magnet ring to simulate, that the magnet becomes lodged at the point while a distal pressure is

applied against the magnet. Fatigue testing on the stent itself has yet to be tested for prolonged measures therefore we have devised a test plan to utilize 4 new linear actuators outfitted with U-blocks which will pinch the four sides of the stent to test its longevity. Lastly, the team has contemplated ways of preventing blood clotting due to the now open interaction between the outer magnet/coil sheath which has been listed as the primary failure mode upon completion of our process failure analysis. One solution included changing from moving magnets to a translational coil sheath so that the magnets remain fixed in some outer body and the inner body moves. This, along with other ideas, have floated the team meetings and remains an unsolved conundrum left to the upcoming engineers and Dr. Tang.

A.



B.



C.
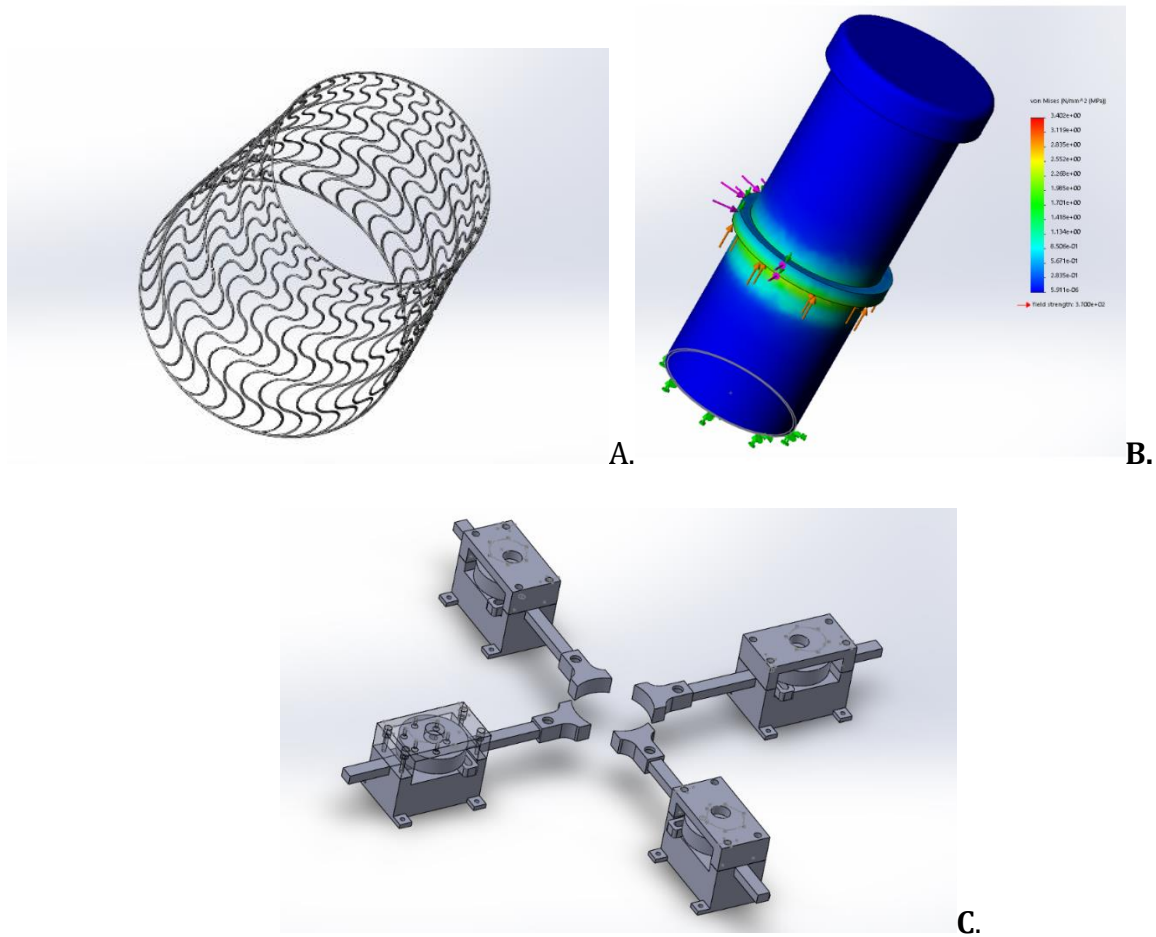
Figure 7-1. Future Work for a Rechargeable Pacemaker.

Where in A, the serpentine stent is shown again as a possible alternative to the diamond cut pattern where the natural design of the struts would allow for potential new elongations versus the current design. B, shows the upcoming study for fatigue against the PDMS/ magnet interface where a fixture is applied to the base of the coil sheath, and the magnet rubs against a fixed point by a distal and inverse normal force to the sheath. C, the design of four linear actuators which will compress the stent simultaneously on the benchtop so that we may examine the design during long term fatigue for 10N-300N forces.

Figure 7-2. Failure Modes and Effect Analysis

| Failure Mode | Failure Effect | Severity | Potential Causes | Occurrence | Current Controls and Detection Method | Detection | Total Risk Score | Action Needed |
|---|---|---|---|---|---|---|---|---|
| Umbrella Mesh Fatigue | Decreased mesh lifespan and failure to oscillate magnet | 7 | Causes include faulty anchoring of mesh and mesh degradation over extended periods of time | 2 | Electrical sensor that relays metrics of the device to a mobile app and notifies user of a critical warning. | 2 | 28 | FEA on mesh to make sure that material can withstand millions of cycles without fracture. |
| Device Endcap Failure | Untethered piece of the device inside the ventricle | 10 | Failure to secure the endcap to the end of the device correctly. | 5 | Patient suffers major internal blockage | 1 | 50 | Design a locking mechanism that will ensure permanent placement of end cap. |
| Magnets get caught on guide rails | No charge produced as magnets are unable to oscillate through the coil | 4 | Improper placing of device in heart leading to different amounts of force around the mesh | 2 | Electrical sensor that relays metrics of the device to a mobile app and notifies user of a critical warning. | 2 | 16 | Research into the properties of a nitinol mesh |
| Recharging device cleaves from pacemaker due to poor anchoring to pacemaker tines | Untethered device inside the ventricle | 10 | Bottom end cap failure | 1 | Patient suffers major internal blockage (probably dies…sad…) | 1 | 10 | Design a locking mechanism that will ensure permanent placement of anchoring site. |

| | | | | | | | |
|---|---|---|---|---|---|---|---|
| Moving magnets interfere with the electronics inside the pacemaker. | Pacemaker is unable to receive charge and pacing is compromised | 8 | Lack of a magnetic shield between magnets and the pacemaker | 1 | Upon installation and use check, pacemaker diagnostics will rend an error warning. | 1 | 8 | Incorporate a magnetic shield into the layered design of the device. |
| Outside magnet does not pull inside magnet | Inside magnet does not move for one cycle lowering efficiency | 2 | Outer diameter magnet is not strong enough | 2 | Set specifications for magnet pull strengths. Ensure that all magnets are verified for pull strength | 1 | 4 | Ensure compatible gauss values for both magnets and make sure outer magnet can pull inner at around 1Hz. |
| Electrical wire line breaks | Incomplete circuit | 7 | Movement of pacemaker/ catheterization damages circuit | 5 | Circuit failure detection | 1 | 35 | none |
| Blood coagulation on guiderails and guide loops | Magnet is not able to move up the guiderails | 8 | Rider mechanism pinches blood cells causing hemorrhaging | 7 | Inner magnet and outer magnet hold the parts from rubbing together | 9 | 504 | Additional Testing needed |
| Electrical wires shorting | Causes electrocution to the nearby area | 6 | Wiring was broken down due to prolonged movement | 4 | Proper installation of the wires prevents the occurrence | 1 | 24 | none |

# Chapter 8 - REFERENCES

[1] K. G. Tarakji, C. R. Ellis, P. Defaye, and C. Kennergren, "Cardiac Implantable Electronic Device Infection in Patients at Risk," *Arrhythmia Electrophysiol. Rev.*, vol. 5, no. 1, p. 65, 2016.

[2] "Medtronic Pacemakers," *Medtronic*. [Online]. Available: https://www.medtronic.com/us-en/patients/treatments-therapies/pacemakers.html. [Accessed: 22-May-2019].

[3] "Tiny pacemaker wows doctors and patients but isn't yet for everyone," *Tampa Bay Times*, 01-Sep-2016. [Online]. Available: https://www.tampabay.com/news/health/tiny-pacemaker-wows-doctors-and-patients-but-isnt-yet-for-everyone/2291942. [Accessed: 22-May-2019].

[4] M. A. Karami, D. J. Inman, and M. Amin Karami, "Powering pacemakers from heartbeat vibrations using linear and nonlinear energy harvesters Modeling and experimental verification of a fan-folded vibration energy harvester for leadless pacemakers Powering pacemakers from heartbeat vibrations using linear," *Cit. Appl. Phys. Lett. Appl. Phys. Rev. J. Appl. Phys. Appl. Phys. Lett. Appl. Phys. Lett. Appl. Phys. Lett.*, vol. 100, no. 101, pp. 42901–41301, 2012.

[5] M. H. Ansari and M. Amin Karami, "Modeling and experimental verification of a fan-folded vibration energy harvester for leadless pacemakers," *J. Appl. Phys. Appl. Phys. Lett.*, vol. 119, no. 100, 2016.

[6] "Atrial Fibrillation Fact Sheet|Data & Statistics|DHDSP|CDC," *Centers for Disease Control and Prevention*. [Online]. Available: https://www.cdc.gov/dhdsp/data_statistics/fact_sheets/fs_atrial_fibrillation.htm. [Accessed: 22-May-2019].

[7] Who Needs Stents and Why?," *Texas Heart Institute*. [Online]. Available: https://www.texasheart.org/heart-health/womens-heart-health/straight-talk-newsletter/who-needs-stents-and-why/. [Accessed: 22-May-2019].

[8] X. Chen, B. Assadsangabi, Y. Hsiang, and K. Takahata, "Enabling Angioplasty-Ready 'Smart' Stents to Detect In-Stent Restenosis and Occlusion," vol. 1700560, pp. 1–10, 2018.

[9] Dilmanian, Hajir, et al. "The Average Stent Length is Longer and the Average Stent Diameter is shorter in Patients with Drug-Eluting Stents versus Bare-Metals Stents During Percutaneous Coronary Intervention." American Journal of Therapeutics. 14(3):277-279, May 2007.

[10] A. L. P. Fenniger, M. A. J. Onsson, A. D. Z. Urbuchen, V. O. M. K. Och, and R. O. L. F. V Ogel, "Energy Harvesting from the Cardiovascular System , or How to Get a Little Help from Yourself," vol. 41, no. 11, pp. 2248–2263, 2013.

[11] Koehler, Kenneth R. College Physics for Students of Biology and Chemistry. Cincinnati, OH: Raymond Walters College University of Cincinnati, 1996: Chapter 3, Fluids: Human Cardiovascular System.

[12] M. H. Ansari and M. A. Karami, "Modeling and experimental verification of a fan-folded vibration energy harvester for leadless pacemakers," *J. Appl. Phys.*, vol. 119, no. 9, 2016.

[13]   W. A. Neill, W. E. Huckabee, L. Art, and P. Art, "Anaerobic Heat Production by the Heart *," vol. 45, no. 9, pp. 1412–1420, 1966.

[14]   D. Press, "Prevention of stent thrombosis : challenges and solutions," pp. 93–106, 2015.

[15]   S. H. Wilson *et al.*, "Infarct artery reocclusion after primary angioplasty , stent placement , and thrombolytic therapy for acute myocardial infarction," 1998.

[16]   Zamir, M. *The Physics of Pulsatile Flow*. AIP Press, 2000.

[17]   "Intracranial artery stenosis, Mayfield Brain & Spine, Cincinnati, Ohio," *mayfieldclinic.com*. [Online]. Available: https://mayfieldclinic.com/pe-intracranialstenosis.htm. [Accessed: 22-May-2019].

[18]   M. Case, M. Micheli, D. Arroyo, J. Hillard "Ultrasonic Blood Flow Sensing Using Doppler Velocimetry,"*International Journal on Smart Sensing and Intelligent Systems.*vol 6. no.4.September 2013

[19]   L.Panwar *et al.*,"Design Of Mems Piezolectric Blood Pressure Sensor,"*IEEE.*vol.no. 2017.

[20]   A. Bussooa, S. Neale, and J. R. Mercer, "Future of Smart Cardiovascular Implants," pp. 1–11, 2018.

[21]   A. You, M. A. Y. Be, and I. In, "Energy harvesting from arterial blood pressure for powering embedded micro sensors in human brain," vol. 124506, no. December 2016, 2017.

[22]   J. E. Lock, *Diagnostic and interventional catheterization in congenital heart disease*. Place of publication not identified: Springer, 2013.

[23]   S. H. Alavi, E. M. Groves, and A. Kheradvar, "The Effects of Transcatheter Valve Crimping on Pericardial Leaflets," The Annals of Thoracic Surgery, vol. 97, no. 4, pp. 1260–1266, 2014.

[24]   M. L. Bernard, "Pacing Without Wires: Leadless Cardiac Pacing," *Ochsner J.*, vol. 16, no. 3, pp. 238–242, 2016.

[25]   "Micra Transcatheter Pacing System Specification Sheet," 2016.

[26]   Donald McLean, John Saunders, "Biologically Implantable and Energized Power Supply", 3563245, 1971

[27]   Sanjay Kotha, T. Sundarshan, R. Radharkishnun, "Magnetic Fluid Power Generator and Method for Generating Power," 6982501, 2006.

[28]   Afraanz Irani, Mark Bianco, David Tran, Peter Deyoung, Melanie Wyld, Tony Li, 'Energy Generating Systems for Implanted medical Devices' 0171404, 2009.

[29]   S. P. Beeby *et al.*, "Measurement Science and Technology Energy harvesting vibration sources for microsystems applications Related content A micro electromagnetic generator for vibration energy harvesting Powering MEMS portable devices—a review of non-regenerative and regenerative," *Meas. Sci. Technol*, vol. 17, pp. 175–195, 2006.

[30]   D. P. Arnold and S. Cheng, "Method and apparatus for motional/vibrational energy harvesting via electromagnetic induction using a magnet array," 0187207, 2015.

[31]   *NASA*. [Online]. Available: https://spinoff.nasa.gov/Spinoff2015/cg_2.html. [Accessed: 22-May-2019].

[32]   Huang, Chuan et.al. "Damping Applications of Ferrofluids: A Review." *Journal of Magnetics*, vol. 22, no. 2, 11 Jan. 2017, pp. 109–121.

[33] A. Bibo, R. Masana, A. King, G. Li, M.F. Daqaq. Electromagnetic Ferrofluid-Based Energy Harvester. *Physics Letters A,* Elsevier. 376, 2163-2166 (2012)

[34] Oh, Dae Woong, et al. "Analysis of Electromotive Force Characteristics and Device Implementation for Ferrofluid Based Energy Harvesting System." *Analysis of Electromotive Force Characteristics and Device Implementation for Ferrofluid Based Energy Harvesting System - IEEE Conference Publication*, ieeexplore.ieee.org/document/7013820/.

[35] J. A. Phys, "Rare earth elements and permanent magnets ( invited )," vol. 721, no. November 2011, pp. 1–7, 2014.

[36] Jayant Sirohi, Inderjit Chopra, "Fundamental understanding of piezoelectric strain sensors," Proc. SPIE 3668, Smart Structures and Materials 1999: Smart Structures and Integrated Systems, (9 June 1999).

[37] Hsu, Jeremy. "Flexible Sensors Measure Blood Flow Under the Skin." *IEEE Spectrum: Technology, Engineering, and Science News*, IEEE Spectrum, 30 Oct. 2015, spectrum.ieee.org/tech-talk/biomedical/devices/flexible-sensors-measure-blood-flow-under-the-skin.

[38] C. Wan and C. Bown, "Multiscale-structuring of polyvinylidene fluoride for energy harvesting: the impact of molecular-, micro- and macro-structure**"** *J. Mater. Chem. A***,** 2017,**5**, 3091-3128

[39] Mohsin Muhyuddin, Aun Nawaz Khan, and Abdul Wadood, "Development and characterization of Nickel–Titanium–Zirconium shape memory alloy for engineering applications," Russian Journal of Non-Ferrous Metals, vol. 58, no. 5, pp. 509–515, 2017.

[40] *Proceedings of the American Power Conference Volume 58-I*. United States: American Power Conference, 1996.

[41] B. Min Yun, C. K. Aidun, and A. P. Yoganathan, "Blood damage through a bileaflet mechanical heart valve: a quantitative computational study using a multiscale suspension flow solver," *J. Biomech. Eng.*, vol. 136, no. 10, p. 101009, Oct. 2014.

[42]  W. D. Fremont, "Corrosion Resistance and Biocompatibility of Passivated NiTi," 2000.

[43] "Friction and Friction Coefficients," *Engineering ToolBox*. [Online]. Available: https://www.engineeringtoolbox.com/friction-coefficients-d_778.html. [Accessed: 23-May-2019].

[44] M. F. Khan, "Design Optimisation for Stent Manufacture," *University of Nottingham.* April, 2018.

[45] J. Kobr *et al.*, "Right Ventricular Pressure Overload and Pathophysiology of Growing Porcine Biomodel," *Pediatr. Cardiol.*, vol. 37, no. 8, pp. 1498–1506, Dec. 2016.

[46] J.Indik , D.Allen , M. Shanmugasundaram, et al."Predictors of resuscitation in a swine model of ischemic and nonischemic ventricular fibrillation cardiac arrest: Superiority of amplitude spectral area and slope to predict a return of spontaneous circulation when resuscitation efforts are prolonged*". *Critical Care Medicine*. 2010;38(12):2352-2357. doi: 10.1097/CCM.0b013e3181fa01ee.

[47] F. S. Angeli *et al.*, "Left ventricular remodeling after myocardial infarction: characterization of a swine  model on beta-blocker therapy.," *Comp. Med.*, vol. 59, no. 3, pp. 272–279, Jun. 2009.

[48] C. M. Tschabrunn *et al.*, "A swine model of infarct-related reentrant ventricular tachycardia: Electroanatomic, magnetic resonance, and histopathological characterization," *Hear. Rhythm*, vol. 13, no. 1, pp. 262–273, Jan. 2016.

[49] R. A. Berg, R. W. Hilwig, K. B. Kern, and G. A. Ewy, "Precountershock cardiopulmonary resuscitation improves ventricular fibrillation median frequency and myocardial readiness for successful defibrillation from prolonged ventricular fibrillation: A randomized, controlled swine study," *Ann. Emerg. Med.*, vol. 40, no. 6, pp. 563–571, Dec. 2002.

[50] M. Argiriou, D. Mikroulis, T. Sakellaridis, V. Didilis, A. Papalois, and G. Bougioukas, "Acute pressure overload of the right ventricle. Comparison of two models of  right-left shunt. Pulmonary artery to left atrium and right atrium to left atrium: experimental study.," *J. Cardiothorac. Surg.*, vol. 6, p. 143, 2011.

[51] S. Gelsomino *et al.*, "Early hemodynamic and biochemical changes in overloaded swine ventricle.," *Texas Hear. Inst. J.*, vol. 40, no. 3, pp. 235–245, 2013.

[52] C. Raoufi, *Applied finite element analysis: with SolidWorks Simulation 2015*. Burnaby, BC: CYRA Engineering Services Inc., 2015.

[53] *KJ Magnets.* [Online]. Available: https://www.kjmagnetics.com/images/blog/article2010.01. [Accessed: 22-May-2019].

[54] M. Hoffman, "Human Heart (Anatomy): Diagram, Function, Chambers, Location in Body," *WebMD*. [Online]. Available: https://www.webmd.com/heart/picture-of-the-heart#1. [Accessed: 22-May-2019].

[55] "Collection of Human Heart Sketch Diagram (41)," *Free Human Heart Sketch Diagram, Download Free Clip Art, Free Clip Art on Clipart Library*. [Online]. Available: http://clipart-library.com/human-heart-sketch-diagram.html. [Accessed: 22-May-2019].